

Self-correcting GKP qubit in a superconducting circuit with an oscillating voltage bias

Max Geier¹ and Frederik Nathan²

¹*Department of Physics, Massachusetts Institute of Technology, Cambridge, MA 02139, USA*

²*NNF Quantum Computing Programme, Niels Bohr Institute, University of Copenhagen, 2100 Copenhagen, Denmark*

(Dated: December 6, 2024)

We propose a simple circuit architecture for a dissipatively error corrected Gottesman-Kitaev-Preskill (GKP) qubit. The device consists of an electromagnetic resonator with impedance $h/2e^2 \approx 12.91 \text{ k}\Omega$ connected to a Josephson junction with a voltage bias oscillating at twice the resonator frequency. For large drive amplitudes, the circuit is effectively described by the GKP stabilizer Hamiltonian, whose low-energy subspace forms the code space for a qubit protected against phase-space local noise. The GKP states in the codespace can be dissipatively stabilized and error corrected by coupling the resonator to a bath through a bandpass filter; a resulting side-band cooling effect stabilizes the system in the GKP code space, dissipatively correcting it against both bit and phase flip errors. Simulations show that this dissipative error correction can enhance coherence time by factor ~ 1000 with NbN-based junctions, for operating temperatures in the $\sim 100 \text{ mK}$ range. The scheme can be used to stabilize both square- and hexagonal-lattice GKP codes. Finally, a Josephson current based readout scheme, and dissipatively corrected single-qubit Clifford gates are proposed.

I. INTRODUCTION

Dissipative quantum error correction (DEC) offers an alternative route to quantum computing, which could bypass the scalability challenges of conventional approaches [1–7]. Leveraging a thermodynamic reservoir to remove noise-induced entropy, DEC can reduce, or completely eliminate, the need for overhead qubits, readout, and feedback control to stabilize quantum information.

While long an elusive goal [4, 8], proposals for genuine DEC—that protects against both phase and bit flip errors—have recently begun emerging in circuit-QED architectures [6, 7]. These approaches use Gottesman-Kitaev-Preskill (GKP) to encode a qubit in charge and phase variables of an electromagnetic resonator [9–11], dissipatively stabilizing it by coupling the resonator to a thermal reservoir and modulating an attached Josephson junction with a periodic driving protocol, either a pulse comb [6] or a stepwise activation protocol [7]. Numerical and analytic results from these works indicate a potential for exponential improvements in qubit stability; at the same time the requirement for high control resolution constitutes an important challenge.

Here, we propose an architecture for dissipatively stabilizing and error correcting a GKP qubit, using only standard circuit elements. The device, shown in Fig. 1(a), consists of an electromagnetic resonator with impedance near $h/2e^2 \approx 12.91 \text{ k}\Omega$, connected through a Josephson junction to an oscillating voltage bias close to resonance with twice the resonator frequency, the effective (Floquet) Hamiltonian of the circuit approaches a GKP stabilizer Hamiltonian whose twofold degenerate low-energy eigenstates are GKP logical states. The GKP states can be dissipatively stabilized by coupling the resonator to a resistor through a detuned lossy resonator or sharp-edge band-pass Purcell filter [12] with bandwidth approximately confined between $1/2$ and $3/4$ of the driving frequency. The coupling induces a side-band

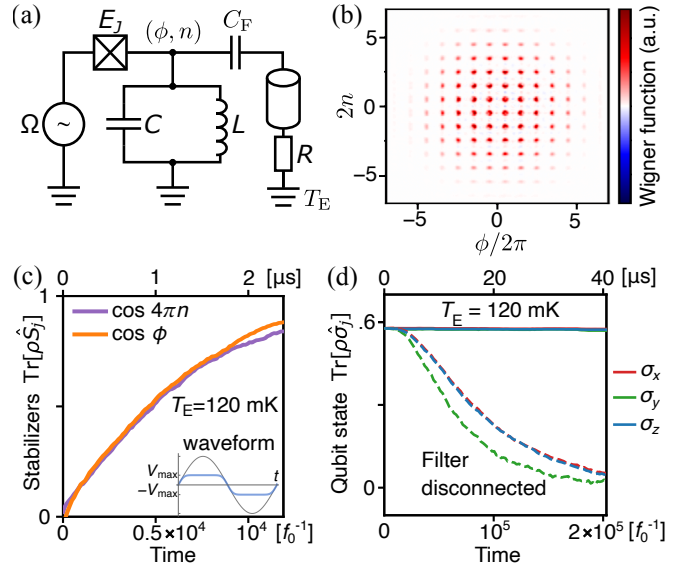


FIG. 1. (a) Circuit diagram for the dissipatively-stabilized GKP qubit. (b) Wigner function for the final state of the resonator and (c) evolution of GKP stabilizers, starting from a high-temperature mixed state. The filter bandwidth and temperature is set to $f/2 \leq f \leq 3f/4$ and temperature $T_E = 120 \text{ mK}$, respectively. (d) Logical information stored in a GKP state initialized in an equal superposition of σ_x , σ_y , and σ_z expectation values with (solid) and without (dashed lines) bandpass filter.

cooling mechanism that can stabilize the system in a GKP state, thereby realizing dissipative error correction. The side-band cooling can stabilize the qubit at a sub-ambient effective temperature [13], allowing operation at the temperature scales up to that of the resonator frequency: our simulations [Fig. 1(b) and (c)] suggest that, for NbN-based junctions, this mechanism can stabilize a random high-energy initial state to a GKP state within

$\sim 2 \mu\text{s}$ at filter temperatures beyond 500 mK while DEC emerges below 200 mK, for a typical resonator frequency $f_0 = 5 \text{ GHz}$. We also discuss how protected Clifford gates can be implemented via appropriate modulation of the oscillating bias, and readout/initialization can be realized via stroboscopic measurement of the supercurrent in an ancilla Josephson junction.

Recently, several works have proposed [7, 14–16] or demonstrated [11, 16–19] new approaches for preparing and stabilizing GKP states, using circuit-QED, or trapped-ion platforms. Besides demonstrated applications for long-coherence qubits [11, 16, 20, 21], these exotic states have been proposed as displacement sensors [22], long-distance quantum communication [23] and as quantum repeaters [24, 25]. They moreover have multiple uses in quantum information processing, including concatenation with other codes for improved error correction [26–28], and interfaces with quantum memories [29]. GKP qubits support natural implementations of Clifford gates [9], while the exploration of non-Clifford gates remains an active research area [6, 30–32]. The approach we present in this paper may provide a relatively simple means for dissipatively generating these exotic and valuable states without need for readout or active feedback control for stabilization.

The remainder of the paper is structured as follows: in Sec. II we summarize our main results. In Sec. III we introduce its self-correcting GKP qubit and discuss its key operating principles, while Sec. IV provides data from numerical simulations. In Secs. V and VI we propose gate and readout/initialization protocols. We conclude with a discussion in Sec. VII.

II. SUMMARY OF MAIN RESULTS

The central developments reported in this article are:

1. The stabilizer Hamiltonian of the square-GKP code, H_{GKP} , can emerge as the effective description of a resonator with impedance $Z = h/2e^2$, when the resonator is connected to an oscillating voltage bias through a Josephson junction. Specifically, H_{GKP} emerges as the effective description of the circuit when the voltage bias oscillates near twice the resonator frequency with an amplitude large relative to the resonator frequency and Josephson energy of the junction. An analogous mechanism can be used to realize the hexagonal GKP code.
2. The low-energy subspace of H_{GKP} , defining the logical codespace of a protected GKP qubit, can be dissipatively stabilized by introducing generic phase-space local dissipation; e.g. by capacitively coupling the resonator to a thermal bath. This principle serves as a means for generation, stabilization, and dissipative quantum error correction of GKP states, protecting against both bit flip and phase errors.

3. Appropriate bath filtering induces a side-band cooling mechanism that may cool the qubit to sub-ambient temperatures, enabling operation and dissipative error correction at high ambient temperature ranges ($\sim 100 \text{ mK}$), set by the resonator frequency ($\sim 5 \text{ GHz}$).

4. Protected Clifford gates can be implemented via appropriate modulation of the oscillating bias, using mechanisms similar to those described in Refs. [7, 10] (see Fig. 4). Due to the self-correcting properties of the qubit, we expect errors from control noise are significantly suppressed due to dissipation with these gate protocols.

We emphasize that the dissipative error correction mechanism we describe protects the qubit against *phase-space local noise*, defined as finite-order polynomial of resonator-mode quadratures. This class of noise includes charge and flux noise, photon loss, and weak control noise. Notably, it does not include quasiparticle poisoning, and hence we expect this noise source to be a limiting factor for our qubit. However, improvements in control of superconducting resonator devices mean that these events can be relatively rare, and potentially easily be mitigated with active error correction [33].

Our analysis indicates that the dissipative processes that error correct the qubit contains weak phase-space non-local contributions from the finite-frequency corrections, giving them a small, but finite, probability of inducing a logical errors. We thus expect a fundamental limit on dissipation-induced lifetime-extension with our scheme, in contrast to the proposal from, e.g., Ref. [7]. At the same time, we emphasize that the lifetime-extension from dissipative error correction can remain significant, due to strong suppression of these processes: our simulations indicate that the dissipative error correction mechanism can potentially extend qubit coherence time by a factor ~ 1000 (see Fig. 3). We also note that the phase-space nonlocality of the dissipative processes will not affect the protocol's utility for generating GKP states.

The operating temperature and driving frequencies of our protocol are limited by the resonator frequency, which in turn must be much smaller than the maximal voltage bias across the junction, V_{max} . This amplitude is in turn limited by the superconducting gap of the Josephson junction, Δ which thereby sets the scale of the operating frequency and temperature of the qubit. For this reason, we suggest NbN as a promising candidate superconductor for our proposal, due to its large superconducting gap and because high-impedance resonators have been demonstrated therein [34]. By optimizing the pulse shape [see inset in Fig. 1(c)] for $V_{\text{max}} = 1.45 \text{ mV}$ (approximately half the $\sim 3 \text{ meV}$ superconducting gap of NbN), we identify an operating regime with $\sim 5 \text{ GHz}$ resonators and bath temperatures in the 100 mK regime.

III. SELF-CORRECTING QUBIT

Here the device and its operating principles are presented.

A. Device

The device consists of an electromagnetic resonator with frequency f_0 and impedance Z . The resonator is connected through a Josephson junction to an oscillating voltage bias $V(t)$ with frequency $f = 1/T$ close to a rational multiple of f_0 . Describing the resonator by its dimensionless phase and number variables, ϕ and $n = -i\partial_\phi$ [35] the circuit Hamiltonian reads

$$H(t) = \frac{hf_0}{2} \left[\frac{\phi^2}{2\pi\zeta} + 2\pi\zeta n^2 \right] - E_J \cos[\phi - \Phi(t)]. \quad (1)$$

where E_J denotes the Josephson energy of the junction, $\zeta \equiv Z/[h/4e^2]$ gives the impedance in units of the quantum resistance, and $\Phi(t)$ denotes the phase induced by the voltage drive, satisfying $\partial_t \Phi(t) = \frac{2e}{\hbar} V(t)$ [36] While our results apply to arbitrary waveforms $V(t)$, we focus for concreteness on a harmonic drive $V(t) = V_0 \sin \Omega t$, with $\Omega \equiv 2\pi f$ the angular drive frequency, such that $\Phi(t) = \frac{2eV_0}{\hbar\Omega} \cos \Omega t$.

B. Dissipative error correction with GKP states

In this paper, we show that the device described by Eq. (1) can stabilize and dissipatively error correct a qubit encoded in GKP states. GKP states have their ϕ - and n -support confined in a characteristic grid, near integer multiples of 2π and $1/2$, respectively; see Fig. 1(b) for an example of a Wigner function [9] [37]. The multiple parities define the σ_z and σ_x logical operators of the qubit:

$$\sigma_z = \Xi(\phi/2\pi), \quad \sigma_x = \Xi(2n), \quad \sigma_y = -i\sigma_x\sigma_z. \quad (2)$$

where the *crenelation function* $\Xi(x) \equiv \text{sgn}(\cos(\pi x))$ indicates the parity of the integer closest to its argument [7, 38][39] Crucially, the encoding above is redundant, allowing a *mixed* resonator state to encode a *pure* logical state [7, 38].

The logical operators $\{\sigma_i\}$ are protected against phase-space local noise, defined as noise generated by finite-order polynomials of ϕ and n , such as, e.g., charge or flux noise, or photon loss: since phase-space local evolution generates a continuous flow of probability densities for both ϕ and n , $\{\langle\sigma_i\rangle\}$ can only change if the distributions acquire support near the domain boundaries of the logical operators, at $\phi \in 2\pi(\mathbb{Z} + 1/2)$ and $n \in \frac{1}{2}(\mathbb{Z} + 1/2)$. DEC can thus be realized if we associate an energy cost with these domain boundaries. This is achieved with the *GKP stabilizer Hamiltonian*,

$$H_{\text{GKP}} = -\varepsilon[\cos(\phi) + \cos(4\pi n)], \quad (3)$$

with ε an arbitrary scale prefactor: the low-energy subspace of H_{GKP} , termed *code subspace*, is given by the mutual high-eigenvalue subspace of the two commuting *GKP stabilizers* $S_1 \equiv \cos(\phi)$ and $S_2 \equiv \cos(4\pi n)$, where the system's probability support in ϕ and n is confined near $\phi \in 2\pi\mathbb{Z}$ and $n \in \mathbb{Z}/2$, away from the boundaries of the logical operators.

In a system described by H_{GKP} , DEC can be achieved by coupling *any* phase-space local observable (such as, e.g., ϕ or n) to a generic thermal reservoir in a system described by H_{GKP} : crucially, the induced dissipation will be *phase-space local*, and moreover stabilize the system in a low-temperature state [40, 41]. The dissipation thereby confines the system deep within the code subspace without affecting the logical information, leading to a dissipatively corrected qubit with strongly enhanced lifetime [7].

C. Emergence of GKP Hamiltonian

Here we show that the GKP Hamiltonian H_{GKP} emerges as the effective Hamiltonian of the device in Eq. (1) when $Z \approx h/2e^2$ and $f \approx 2f_0$, and $V_0 \gg E_J/2e, hf/2e$.

We demonstrate the emergence of H_{GKP} by eliminating the fast degrees of freedom to obtain an effective low-energy Hamiltonian for the resonator [42–44]: we consider the evolution of the system in a comoving frame of phase space that rotates uniformly with angular frequency $\tilde{\Omega} = \Omega/2$ [45], coinciding with the original lab frame at $t = z\tilde{T}$ for $z \in \mathbb{Z}$, with $\tilde{T} \equiv 2\pi/\tilde{\Omega} = 2T$. Evolution in the rotating frame is generated by the Hamiltonian $\tilde{H}(t) = H_d - E_J \cos[\phi \cos \Omega t - 2\pi\zeta n \sin \tilde{\Omega} t - \frac{2eV_0}{\hbar\omega_0} \cos 2\tilde{\Omega} t]$ where $H_d \equiv \frac{hf_0}{2}(\phi^2/2\pi\zeta + 2\pi\zeta n^2)$ and $\delta f \equiv f_0 - f/2$ denotes the frequency detuning from resonance [42–44]. The Hamiltonian $\tilde{H}(t)$ is explicitly time-periodic with a *doubled* period, $\tilde{T} \equiv 2T$. The evolution in the rotating—and hence also lab—frame at integer multiple of \tilde{T} are equivalent to those generated by the *effective Hamiltonian* $H_{\text{eff}} \equiv i \log U(\tilde{T})/\tilde{T}$ where $U(t) \equiv \mathcal{T} e^{-i \int_0^t \tilde{H}(t) dt}$ with \mathcal{T} the time-ordering symbol, and the logarithm branch cut is defined from analytic continuation from zero.

For $V_0 \gg E_J/2e$, Cooper pair tunneling through the Josephson junction is effectively blocked away from the nodes of the voltage signal, which are located at $t \in \frac{T}{2}\mathbb{Z}$: away from these nodes, the voltage bias generates a fast oscillation of the second term in $\tilde{H}(t)$, effectively averaging the Josephson coupling to zero. This allows us obtain H_{eff} via a combination of a rotating wave and stationary phase approximation (see App. A), resulting in H_{eff} given by a weighted average of $\tilde{H}(t)$ at the nodes of the voltage oscillation, $t \in \frac{T}{2}\mathbb{Z}$:

$$H_{\text{eff}} \approx \frac{hf_0}{2} \left(\frac{\phi^2}{2\pi\zeta} + 2\pi\zeta n^2 \right) - \tilde{E}_J [\cos \phi + \cos 2\pi\zeta n] \quad (4)$$

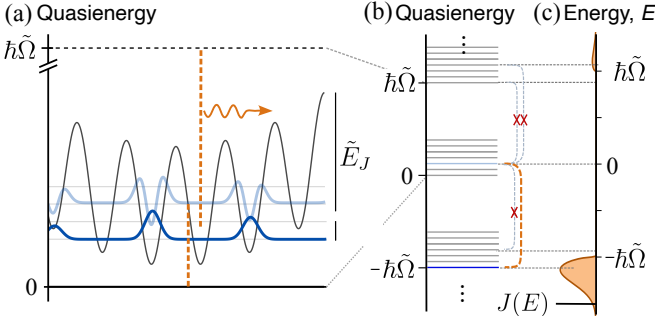


FIG. 2. **Sideband-cooling-enabled dissipative error correction.** (a) A cooling transition between two GKP states can be generated by emission of a photon at energy $\hbar\tilde{\Omega} + \Delta\varepsilon$, with $\Delta\varepsilon$ the characteristic excitation energy of H_{eff} [Eq. (4)]. (b) Dissipative error correction, that relax energy in the GKP subspace, emerges when dissipation is dominated by such processes. This can be achieved with a filtered bath whose spectral function $J(E)$ has support concentrated in the interval $E \in [\hbar\tilde{\Omega}, 1.5\hbar\tilde{\Omega}]$ as shown in (c). Here, $J(E)$ is shown for system parameters from Table I with $T_E = 120$ mK.

with $\tilde{E}_J = \frac{E_J \cos(\Phi(0) - \pi/4)}{T \sqrt{\zeta e |V'(0)|/h}}$ (see App. A). For $h\delta f \ll \tilde{E}_J$, and $\zeta \approx 2$, we see that H_{eff} becomes identical to H_{GKP} . Importantly, perturbative arguments show that the low-energy subspace of H_{eff} remains confined in the GKP code subspace even when accounting for finite, small detunings δf and finite drive frequencies (see App. A).

Our analysis can be generalized to more general waveforms $V(t)$, and that stabilizer Hamiltonians of different GKP encodings can be realized for different choices of waveforms and resonator impedances. In particular, the stabilizer Hamiltonian of a z -dimensional GKP qudit can be realized in a similar fashion as above when $\zeta \approx z$ for any integer z . In App. A, we demonstrate that the stabilizer Hamiltonian of a hexagonal GKP qubit emerges for $\Omega \approx 3\omega_0$, $\zeta \approx 4/\sqrt{3}$. Hexagonal GKP codes may have advantageous error correction properties over the square GKP code [46].

D. Dissipative error correction from filtered bath

We now show the circuit can be dissipatively stabilized and error corrected by capacitatively connecting the resonator to a thermal reservoir with constrained spectral density [47], such as a resistor connected through a dissipative resonator [48] or band-pass filter [12], as shown in Fig. 1 [49]. The capacitatively-coupled resistor is modeled as $H_{\text{RC}} = \frac{2enq_B(t)}{C_B}$, where $q_B(t)$ denotes the fluctuating charge on the resistor-side of the coupler, and C_B the capacitance of the coupler. The bath variable $B(t) = 2eq_B(t)/C_B$ is modeled as a quantum noise variable with equilibrium power spectral density $J(E)$. Here $J(E)$ can be obtained by weighing the spectral density of B determined by the filter, $S(E)$, [50]: $J(E) = S(|E|)[\theta(E) + n_B(|E|)]$, as with θ denoting the

Heaviside step function.

We model the dissipative dynamics of the circuit via a jump operator through the universal Lindblad formalism from Refs. [40, 51–54], which is valid when the resistor-induced loss rate is much smaller than the inverse correlation time of resistor fluctuations [40, 54]. In App. D, we show that, in this limit, and for $f \gg \tilde{E}_J/h, \delta f$, the stroboscopic dynamics within the code subspace becomes approximately equivalent to those generated by the *time-independent* master equation.

$$\partial_t \rho(t) = i[\rho(t), H_{\text{eff}}] + \sum_{z=-\infty}^{\infty} \left(L_z \rho(t) L_z^\dagger - \frac{1}{2} \{L_z^\dagger L_z, \rho(t)\} \right). \quad (5)$$

Here L_z is constructed from the eigenvalues $\{\varepsilon_a\}$ and eigenstates $\{|\psi_a\rangle\}$ of H_{eff} (the former defined via continuation from the high-frequency limit) through

$$L_z = \sum_{ab} \sqrt{2\pi J(\varepsilon_b - \varepsilon_a + z\hbar\tilde{\Omega})} |\psi_a\rangle \langle \psi_a| \bar{n}_z |\psi_b\rangle \langle \psi_b|,$$

where $\bar{n}_z \equiv \frac{1}{T} \int dt \mathcal{M}^\dagger(t) [n \cos \tilde{\Omega}t + \phi \sin \tilde{\Omega}t] \mathcal{M}(t) e^{-iz\tilde{\Omega}t}$ and $\mathcal{M}(t) \equiv U(t) e^{iH_{\text{eff}}t} = \mathcal{M}(t + \tilde{T})$ denotes the time-periodic micromotion operator of the system, which approaches the identity in the rapid-driving limit [55]. The jump operator L_z describes side-band incoherent processes involving the absorption of z photons of the period-doubled drive signal defined by $\tilde{H}(t)$ [56]. In the rapid-driving limit, where $\mathcal{M} \approx 1$, \bar{n}_z is only significant for $z = \pm 1$, reflecting that processes involving the emission/absorption of a single resonator photon dominate relaxation dynamics, if admitted by the bath.

The evolution generated by Eq. (5) is equivalent to that of a nondriven system described by H_{eff} connected to an array of thermal baths with power spectral densities $\{J(E + z\hbar\tilde{\Omega})\}$ for $z \in \mathbb{Z}$ via the terms \bar{n}_z [40]. The system can be relaxed into the code subspace via sideband cooling [13] if $k_B T_E \ll h\tilde{f}$, if the bath effectively only admits modes with energies within the window $[\hbar\tilde{\Omega}, 3\hbar\tilde{\Omega}/2]$, as can e.g. be realized with Purcell filters [48] or superconducting metamaterials [12]. In this case, only L_1 is effectively nonzero, reflecting that the filtered bath only admits relaxation processes involving the emission of a single resonator photon. Consequently, the system for transitions at energy difference ΔE , $T_{\text{eff}} = \frac{2\Delta E}{k_B} \frac{J(\hbar\tilde{\Omega} + \Delta E)}{J(\hbar\tilde{\Omega} - \Delta E/h)}$ is given by

$$T_{\text{eff}}(\Delta E) \approx \frac{\Delta E/k_B}{\log S(\hbar\tilde{\Omega} + \Delta E) - \log S(\hbar\tilde{\Omega} - \Delta E)} \quad (6)$$

where we used $J(E) \approx S(E)$ for $E \gg k_B T_E$. If $S(E)$ changes appreciably (in relative terms) from $\hbar\tilde{\Omega} - \Delta\varepsilon$ to $\hbar\tilde{\Omega} + \Delta\varepsilon$, with $\Delta\varepsilon \sim (\tilde{E}_J h \delta f)^{1/2}$ the characteristic excitation energy of H_{eff} [7], the effective temperature experienced by the resonator can be much smaller than \tilde{E}_J , implying that the bath effectively cools the resonator into the low-energy subspace of \tilde{H}_{eff} , i.e., the code subspace [see Fig. 2]. Moreover, since \bar{n}_z is approximately

close to $n_1 \approx \frac{1}{2}\phi - iq$ in the high-frequency limit (where $\mathcal{M}(t) \approx 1$ [55]), the term generating the relaxation is phase-space local. As a consequence, this relaxation mechanism has a very low probability to induce logical errors due to the disjoint wavefunction of GKP states. Hence, the dissipative stabilization into subspace will not affect the logical information encoded in our qubit, implying that our scheme realizes dissipative error correction.

Note that the stabilizing jump operator L_1 generically contains small, phase-space non-local contributions from the finite-frequency corrections to \bar{n}_1 [55]. The dissipative error correction process generated by L_1 hence has a small, but finite, probability of inducing a logical error, even while stabilizing states into the GKP code subspace. We thus expect a fundamental upper bound on dissipation-induced lifetime-extension with our scheme, contrasting to the proposal from, e.g., Ref. [7]. At the same time, we stress that the lifetime-extension can remain significant, due to the strongly suppressed (though nonzero) amplitude for micromotion-dressed processes: for the parameters in Table I, we numerically estimate a typical error probability of $|\langle L_1^\dagger \sigma_z L_1 \rangle / \langle L_1^\dagger L_1 \rangle - \langle \sigma_z \rangle| \approx 10^{-4}$ for excited GKP states in the code subspace. Indeed, our numerical simulations (Sec. IV) show that dissipation can potentially extend lifetime of the qubit by a factor ~ 1000 (see Fig. 3).

We finally note that the phase-space nonlocality of L_1 will not affect the protocol's utility for generating GKP states.

The side-band cooling mechanism above is not the only way to achieve dissipative error correction: an alternative approach, which does not require sharp edges of bath spectra, is to operate the system with a low-pass filter; we discuss this approach in more detail in App. F. The low-pass filter approach relies on direct cooling without resonator photon emission (rather than side-band cooling), thus requiring bath temperatures much smaller than \bar{E}_J . We find a reasonable parameter regime for the approach with NbN-based Josephson junctions, where stabilization of GKP states occurs below 40mK and dissipative error correction sets in below 20mK [see App. F for further details].

IV. NUMERICAL SIMULATIONS

We simulate the stroboscopic dynamics of the circuit with $\zeta = 2$, $f \approx 2f_0$, and a bandpass filter with bandwidth confined between $1/2$ and $3/4$ of the driving frequency. We numerically integrate Eq. (5) via the stochastic Schrödinger equation [57, 58], using 1000 realizations per parameter set. We obtain H_{eff} exactly from $\frac{i}{T} \log \mathcal{T} e^{-i \int_0^T H(t) dt}$, discretizing the Hilbert space via a regularly-spaced ϕ grid [59], and compute the jump operators $\{\bar{L}_z\}$ via the expression below Eq. (5). Noting that the jump operators are not sensitive to the specific details of the spectral function as long as the support is

f_0	δf	E_J/h	$\Gamma_{\bar{a}}/2\pi$	κ	Λ_B	T_E	V_{max}
5 GHz	6 MHz	20 GHz	5 kHz	.002	.35 GHz	.05 K	1.45 mV
-	.0012 f_0	4.0 f_0	$10^{-6} f_0$.002	.07 f_0	.2 f_0	70 f_0

TABLE I. *Row 1*: Default parameters for simulations. Here, f_0 denotes the resonator frequency, δf the detuning of drive frequency from $2f_0$, E_J the junction Josephson energy, $\Gamma_{\bar{a}}$ the extrinsic photon loss rate, κ the dimensionless system-bath coupling, Λ_B filter bandwidth, T_E resistor temperature, and V_{max} voltage amplitude. See App. E and inset in Fig. 1(c) for explicit waveform. The resonator frequency corresponds to inductance $L = 410$ nH and capacitance $C = 2.5$ fF. *Row 2*: parameter values in terms of the resonator frequency, f_0 , in units where $h = e = k_B = 1$, enabling extension to other parameter sets via rescaling.

confined within the interval $[\hbar\tilde{\Omega}, 3\hbar\tilde{\Omega}/2]$, we model the filtered spectral function for $E > 0$ as

$$J(E) = \kappa \theta(E - \hbar\tilde{\Omega})(E - \hbar\tilde{\Omega}) e^{-\frac{(E - \hbar\tilde{\Omega})^2}{2\Lambda_B^2}}, \quad E > 0 \quad (7)$$

For $E < 0$, we define $J(E)$ from $J(-E)$ via the detailed balance condition $J(-E) = e^{-E/k_B T_E} J(E)$ [50]; see Fig. 2(c) for a plot of $J(E)$ with $T_E = 120$ mK and $\Lambda_B = 0.07\hbar f_0$. The filter has a sharp lower cut-off at $\hbar\tilde{\Omega}$ to allow for photon-assisted relaxation processes while suppressing any bath-induced excitations in the GKP subspace. To demonstrate the system's resilience to noise we also include extrinsic photon loss in the simulation through an additional jump operator $\hat{a} = \sqrt{\pi}\Gamma_a\zeta(\phi - in/2\pi\zeta)$ in the lab frame (see App. D for details); here Γ_a denotes the loss rate.

We use default parameters that we expect are feasible for NbN superconductors with gap $\Delta_0 = 3$ meV [60], listed in Table I. We use a driving tone containing a superposition of sinewaves at the 7 lowest odd harmonics of the fundamental frequency $f = 2f_0 + \delta f$, with amplitude V_{max} and nodal slope $V'(0) = 2.94 \times 2\pi f V_{\text{max}}$ (see inset in Fig. 1(c) and App. E); the waveform is chosen together with E_J to maximize the barrier height of the effective potential, \tilde{E}_J without invalidating the effective description of the circuit in terms of H_{GKP} . The parameters and waveform above result in $\tilde{E}_J/h \approx 0.11f_0 \approx 0.55$ GHz

We first demonstrate the dissipative stabilization of GKP states by our scheme. To this end, we evolve a generic high-temperature initial state [61] over a time interval $12000/f_0 \approx 2.4 \mu\text{s}$ at resistor temperature $T_E = 120$ mK. Figs. 1(b,c) show the resulting Wigner function of the final state (b) and evolution of GKP stabilizers (c). Evidently, the system relaxes to a GKP state within $\sim 2 \mu\text{s}$. Fig. 1(d) shows the evolution of the logical operators $\{\sigma_i\}$ defined in Eq. (2), in the presence and absence of dissipation. Evidently, the dissipation leads to a significant improvement of the qubit lifetime. The halved lifetime of σ_y relative to those of $\sigma_{x,z}$ is consistent with the dominant error processes being caused by transitions across the potential energy barriers of H_{GKP} —located at $\phi \in 2\pi\mathbb{Z}$ and $n \in \frac{1}{2}\mathbb{Z}$. These transitions will result in

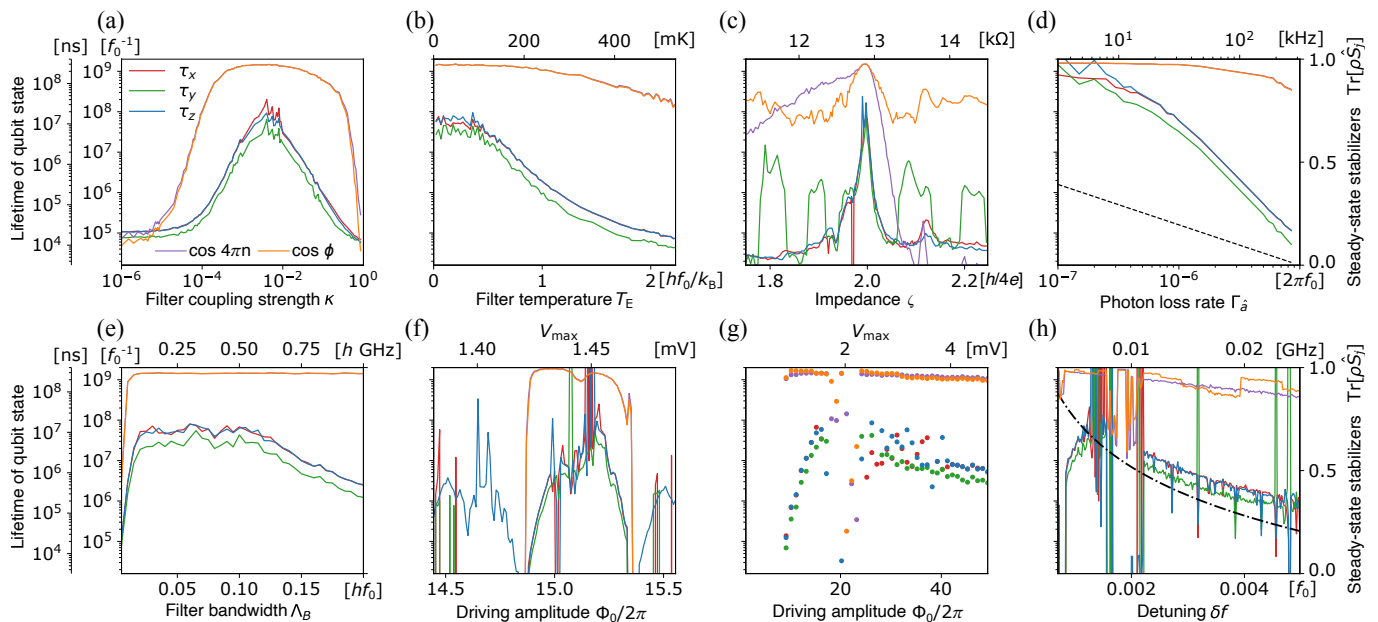


FIG. 3. **Numerical results.** Lifetimes of information τ_j , $j = x, y, z$ stored in the expectation values of the logical operators $\langle \hat{\sigma}_j \rangle$, $j = x, y, z$ and steady-state stabilizer expectation values as a function of (a) dimensionless coupling to the filtered bath, (b) temperature (c) impedance, (d) photon loss rate, (e) filter bandwidth, (f) driving amplitude, (g) driving amplitude at maxima $\Phi_0 = 2\pi(z + 0.2)$, $z \in \mathbb{N}$, and (h) detuning. We keep all non-varied parameters fixed at the default values in Table I.

error processes generated by σ_x and σ_z at equal rates.

In Fig. 3, we plot the qubit lifetimes and stabilizer expectation values as a function of the most relevant device parameters [62].

Illustrating the role of dissipation for stabilizing the qubit, Fig. 3(a) shows that qubit lifetime and stabilizer expectation values grows with system-bath coupling κ , for $\kappa \gtrsim 10^{-4}$. The onset of stabilization at $\kappa \approx 10^{-4}$ marks the point where the stabilization time of GKP states matches the photon loss time. For $\kappa \gtrsim 10^{-2}$, lifetime begins to decrease again; we expect this to be due to the proliferation of logical errors caused by the non-locality of the jump operators, discussed below Eq. (5). Fig. 3(b) shows that stabilization of GKP states occurs for temperatures $T_E \lesssim 4hf_0/k_B \approx 1$ K, while DEC emerges for $T_E \lesssim hf_0/k_B \approx 250$ mK. As T_E is decreased below this threshold, lifetime appears to increase exponentially. For deviations of the resonator impedance from $h/2e^2$ [Fig. 3(c)], our simulations indicate a narrow relative tolerance of $\approx 0.5\%$ for DEC while stabilization of GKP states has a significantly larger tolerance for deviations of the impedance, of order $\approx 10\%$.

As a function of photon loss rate [Fig. 3(d)], stabilization of GKP states sets in when the time between two photon loss events $1/\Gamma_{\hat{a}}$ becomes longer than the time it takes to stabilize the GKP states, t_{stab} ; for the parameters we use (see Table I), $t_{\text{stab}} \approx 10000f_0^{-1}$ [compare Fig. 1(c)]. Lifetime enhancement appears to saturate for $\Gamma_{\hat{a}}/2\pi \lesssim 10^{-6}f_0$.

For our chosen filter spectral function with lower threshold for support fixed to $\hbar\tilde{\Omega}$ [see Eq. (7)], the life-

time exhibits a plateau as a function of the upper boundary of the band, Λ_B [Fig. 3(e)], as long as Λ_B (i) is sufficiently small to prohibit processes where two resonator photons are absorbed by the bath in combination with an excitation in the effective potential described by $H_{\text{eff}}(\Lambda_B \ll hf_0)$ and (ii) sufficiently large to allow relaxation of the GKP states within the code space, i.e., larger than the characteristic excitation energy of H_{eff} , $\Delta\varepsilon$. The plateau demonstrates that the results do not depend on the precise shape of the filter spectral function, as long as the main qualitative features are preserved (threshold above $E = \hbar\tilde{\Omega}$, bandwidth smaller than $\hbar\tilde{\Omega}/2$).

We next consider the roles of the waveform parameters. In Figs. 3(f) we plot lifetime and stabilizer expectation value against bias amplitude V_{max} , in a window [1.38 mV, 1.49 mV]. Evidently, these quantities exhibit a significant dependence on V_{max} in this window. The lifetimes peaks close to $2\pi z + \pi/4$, $z \in \mathbb{N}$ where the GKP potential Eq. (4) is positive and the GKP states are centered around $\phi = 2\pi k + \pi$ and $n = k/2 + 1/4$, $k \in \mathbb{Z}$ so that the logical sectors are related by a phase-space inversion $\phi \rightarrow -\phi$, $n \rightarrow -n$. In this configuration, the GKP states are degenerate also in the presence of the quadratic confinement due to the detuning, c.f. Eq. (4). The shown pattern is repeated as V_{max} is increased beyond this window, consistent with the effective barrier height being 2π -periodic in the phase oscillation amplitude, Φ_0 [see Eq. (4)]. We next compute the stabilizer expectation values and lifetimes for a broader range of values of V_{max} , each picked at $\Phi_0 = 2\pi(z + 0.2)$, $z = 1, 2, 3$, close to the local optimum over the oscillation [Fig. 3(g)].

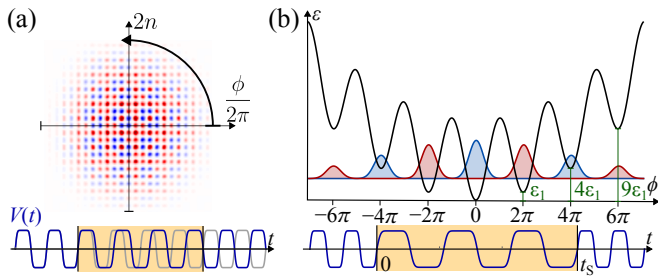


FIG. 4. **Protected single-qubit Clifford gates.** (a) A protected Hadamard gate, expressed as a $\pi/2$ rotation in phase space, is performed by a π phase shift of the voltage pulse (blue) relative to normal operation (gray). (b) A protected S -gate is performed by switching to a driving frequency close to the resonance frequency f_0 and then letting even and odd wells acquire a relative $\pi/2$ phase shift from dynamic phases $k^2 \varepsilon_1 t / \hbar$ of well k with $\varepsilon_1 = \frac{\pi}{2} \hbar \delta f'$.

Evidently, beyond a minimal threshold required for stabilization, corresponding to $\Phi_0 \gtrsim 20\pi$, lifetime decreases with V_{\max} , consistent with our expectation that the effective GKP barrier height \tilde{E}_J scales as $|V'(0)|^{-1/2} \propto V_{\max}^{-1/2}$ [see Eq. (4)].

In Fig. 3(h), we consider the role of frequency detuning δf : we find that lifetime is maximized at $\delta f_{\text{opt}} \approx .0012 f_0$. Larger δf leads to lifetime decreasing, because the resulting GKP squeezing parameter $\lambda \propto (\delta f / \tilde{E}_J)^{1/4}$ increases, enhancing the error rate due to interwell-tunneling [7]. Decreasing δf from δf_{opt} leads to lifetime decrease due to the wavefunction envelope ($\propto \lambda^{-1}$) expanding into regions of phase space where finite-frequency corrections to Eq. (4) become important. Varying δf takes the system through narrow resonances, where stabilization breaks down due to hybridization of stabilized GKP states with high-energy levels. We attribute the unstable behavior around $\delta f = 0.0018 f_0$ to hybridization from such resonances. These resonances occur in a low-measure region of detuning, and we expect they can be avoided by appropriate frequency tuning.

V. PROTECTED SINGLE-QUBIT CLIFFORD GATES

For the square GKP code, a Hadamard (H) gate operation $\sigma_H \equiv \frac{1}{\sqrt{2}}(\sigma_x + \sigma_z)$ is generated by a $\pi/2$ phase space rotation. Such an operation can be implemented in the circuit by adiabatically shifting the phase of the voltage tone by π , see Fig. 4(a). Provided the phase shift is sufficiently slow, the system will remain confined in the low-energy subspace of the H_{eff} , implying strong error suppression.

A protected S gate, $e^{-i\frac{\pi}{4}\sigma_z}$, can be implemented using the phase-revival mechanism described in Ref. [7]. The protocol involves the following steps [see Fig. 4(b) and App. B for details]: first, adiabatically turn on an additional driving tone at $\tilde{\Omega}$ so that $\Phi(t) \rightarrow \Phi(t) + \pi \cos \tilde{\Omega} t$.

This adiabatically shifts the minima of H_{eff} by $\Delta\phi = \pi$, so that $|0\rangle$ and $|1\rangle$ GKP logical states have support centered around $\phi \in 4\pi\mathbb{Z}$ and $\phi \in 4\pi(\mathbb{Z} + 1/2)$, respectively. Second, abruptly shift to a driving frequency at $f' = f_0 + \delta f'$ and voltage amplitude so that $\Phi_0 = 2\pi k - 3\pi/4$ and the minima of the potential remain at $\phi \in 2\pi\mathbb{Z}$. This turns off the term $\propto \cos(2\pi\zeta n)$ in H_{eff} stabilizing inter-well phase coherence; allowing for a relative phase accumulation between the two logical sectors. Then, by waiting a time $\Delta t_S = \frac{1}{2\pi\delta f'}$, states with support near $\phi = 2\pi k$ have acquired a phase factor $e^{-ik^2 2\pi^2 \delta f' t_S / 2}$, which takes value $(-i)^{k^2}$; this is equivalent to the action of *i.e.* an S -gate operation. Finally, quenching back to the resonantly modulated driving tone and adiabatically turning off the modulation at frequency $\tilde{\Omega}$, reactivates the interwell-coherence stabilizing term $\propto \cos(2\pi\zeta n)$, which will correct small relative phase errors from a non-perfect waiting time t_S . See also App. B for further details.

VI. READOUT

The logical state of the GKP qubit can be read from the mean supercurrent across a weak Josephson junction J' between a node halfway along the inductance of the resonator and a node [see Fig. 5(a)] driven by a second voltage signal, $V_R(t)$. The voltage tone $V_R(t)$ should have frequency $f_R = f/4$ and (similar to the main-junction driving tone $V(t)$ stabilizing the GKP states) a large voltage amplitude $\max V_R(t) \gg \hbar f_R, E'_J$. The attachment of J' halfway along the inductance means that the Josephson current through J' , is proportional to $\sin \phi/2$ (in the lab frame). The large bias amplitude across J' moreover ensures that the mean current through J' only gets significant contributions near the nodes of $V_R(t)$, which are located at times $t \in \mathbb{Z}\tilde{T}$. The mean supercurrent of the biased junction hence is proportional to the mean value of the stroboscopic evolution of $\sin(\phi/2)$. As a consequence, the logical $|0\rangle$ and $|1\rangle$ states, whose stroboscopic evolutions are confined near $\phi = 2\pi[\mathbb{Z} + 1/2]$ and $2\pi[\mathbb{Z} - 1/2]$, respectively, result in oppositely-valued supercurrents [see Fig. 5(b)]. The readout process can also be applied for initialization. Further details are contained in App. C.

VII. DISCUSSION

In this paper, we proposed a protocol for dissipative stabilizing and error-correcting a GKP qubit in a resonator driven by an oscillating voltage bias through a Josephson junction: First, we showed that the GKP Hamiltonian emerges as the effective description of the circuit for driving near a rational multiple of the resonator frequency. Second, we showed that coupling the resonator to a filtered bath with sharp threshold at half the driving frequency leads to a photon-assisted side-

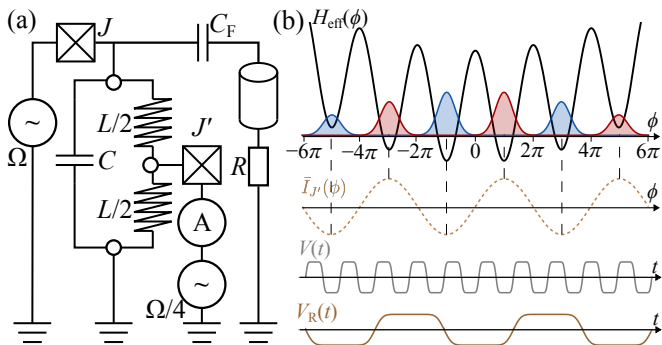


FIG. 5. **Readout.** (a) The readout signal is given the mean supercurrent $\bar{I}_{J'}$, measured through a weak Josephson junction J' connected to the resonator at $L/2$ of its inductance and driven at $\Omega/4$. (b) This yields an effective 4π -periodic potential so that even wells yield $\bar{I}_{J'} = \bar{I}_0$ while odd wells yield $\bar{I}_{J'} = -\bar{I}_0$.

band cooling of the system; this drives the circuit into low-energy GKP states that form the code subspace of a protected qubit, without affecting the encoded logical information. Thereby, this cooling mechanism realizes dissipative error correction. Our simulations demonstrate significant potential for lifetime enhancement, and operating regimes at moderate temperatures (~ 100 mK). At lower temperatures, the circuit may operate with alternative bath low-pass filter configurations that do not involve sharp cutoffs (see App. F). We finally proposed protected single-qubit Clifford gate and readout protocols for the qubit. Our system is compatible with the magic-gate and two-qubit-gate proposals from Ref. [6]; thus complementing a universal gate set.

We expect the circuit can be realized with NbN-based Josephson junctions where a superconducting gap of $\Delta = 3$ meV is typical and superinductors with impedance of $h/4e$ were demonstrated [34]. The dissipative stabilization of GKP states only involves a microwave voltage bias tone, and Purcell or bandpass filter to avoid photon-assisted heating in the GKP subspace; such filters may

be realized in superconducting circuits with lossy resonators [48] or quantum metamaterials [12].

While our protocol can correct against phase-space local noise sources, such as photon loss, phase-space *non-local* noise source, such as tunneling of quasiparticles over the Josephson junction, may limit the lifetime by inducing a random-angle finite phase-space displacements that potentially cause logical errors. We expect the noise source can be mitigated by concatenation with an error-correcting code; since quasiparticle poisoning events can potentially be relatively rare (with rates in the kHz range [33]), potentially simplifying such a scheme. Another important question the role of additional resonator modes (coupled to the qubit mode via the nonlinear Josephson junction). Finally, we expect understanding the role of non-Markovian effects will be important, as these may play a significant role for stronger system-filter coupling due to the constrained support of its spectral functions.

We speculate the device might find use in a quantum information processing architecture due to its simplicity, stability, and support of native, fault tolerant gate operations and readout scheme. Exploring further enhancement of lifetime, along with protocols for multi-qubit [27] and magic gates will be important directions for future studies.

Acknowledgements.— We gratefully acknowledge insightful discussions and collaboration on related projects with Gil Refael, Liam O'Brien, and Matthew H. Matheny. We also acknowledge useful discussions with Karsten Flensberg, Anders Sørensen, Jacob Hastrup, Margarita Davydova, Liang Fu, Virgil Baran, Jonathan Conrad, Max Hays, Lev Arcady-Sellem, and Philippe Campagne-Ibarcq. This work made use of resources provided by subMIT at MIT Physics. M.G. acknowledges support from the German Research Foundation under the Walter Benjamin program (Grant Agreement No. 526129603) and by the Air Force Office of Scientific Research under award number FA2386-24-1-4043. F.N. gratefully acknowledges support from the Carlsberg Foundation, grant CF22-0727.

-
- [1] J. P. Barnes and W. S. Warren, Physical Review Letters **85**, 856 (2000), publisher: American Physical Society.
 - [2] F. Verstraete, M. M. Wolf, and J. Ignacio Cirac, Nature Physics **5**, 633 (2009).
 - [3] H. Bombin, R. W. Chhaajlany, M. Horodecki, and M. A. Martin-Delgado, New Journal of Physics **15**, 055023 (2013), publisher: IOP Publishing.
 - [4] B. J. Brown, D. Loss, J. K. Pachos, C. N. Self, and J. R. Wootton, Reviews of Modern Physics **88**, 045005 (2016), arXiv:1411.6643 [cond-mat, physics:quant-ph].
 - [5] F. Reiter, A. S. Sørensen, P. Zoller, and C. A. Muschik, Nature Communications **8**, 1822 (2017).
 - [6] L.-A. Sellem, A. Sarlette, Z. Leghtas, M. Mirrahimi, P. Rouchon, and P. Campagne-Ibarcq, arXiv 10.48550/arXiv.2304.01425 (2023), 2304.01425.
 - [7] F. Nathan, L. O'Brien, K. Noh, M. H. Matheny, A. L. Grimsmo, L. Jiang, and G. Refael, arXiv 10.48550/arXiv.2405.05671 (2024), 2405.05671.
 - [8] M. J. Kastoryano, L. B. Kristensen, C.-F. Chen, and A. Gilyén, arXiv 10.48550/arXiv.2408.14970 (2024), 2408.14970.
 - [9] D. Gottesman, A. Kitaev, and J. Preskill, Phys. Rev. A **64**, 012310 (2001).
 - [10] P. Campagne-Ibarcq, A. Eickbusch, S. Touzard, E. Zalts-Geller, N. E. Frattini, V. V. Sivak, P. Reinhold, S. Puri, S. Shankar, R. J. Schoelkopf, L. Frunzio, M. Mirrahimi, and M. H. Devoret, Nature **584**, 368 (2020).
 - [11] D. Lachance-Quirion, M.-A. LEMONDE, J. O. Simoneau, L. St-Jean, P. Lemieux, S. Turcotte, W. Wright, A. Lacroix, J. Fréchet-Viens, R. Shillito, F. Hopf-

- mueller, M. Tremblay, N. E. Frattini, J. Camirand Lemyre, and P. St-Jean, *Phys. Rev. Lett.* **132**, 150607 (2024).
- [12] V. S. Ferreira, J. Banker, A. Sipahigil, M. H. Matheny, A. J. Keller, E. Kim, M. Mirhosseini, and O. Painter, *Phys. Rev. X* **11**, 041043 (2021).
- [13] S. Stenholm, *Rev. Mod. Phys.* **58**, 699 (1986).
- [14] J. Conrad, *Phys. Rev. A* **103**, 022404 (2021).
- [15] X. C. Kolesnikow, R. W. Bomantara, A. C. Doherty, and A. L. Grimsmo, *Phys. Rev. Lett.* **132**, 130605 (2024).
- [16] P. Campagne-Ibarcq, A. Eickbusch, S. Touzard, E. Zalts-Geller, N. E. Frattini, V. V. Sivak, P. Reinhold, S. Puri, S. Shankar, R. J. Schoelkopf, L. Frunzio, M. Mirrahimi, and M. H. Devoret, *Nature* **584**, 368 (2020).
- [17] C. Flühmann, T. L. Nguyen, M. Marinelli, V. Negnevitsky, K. Mehta, and J. P. Home, *Nature* **566**, 513 (2019).
- [18] B. de Neeve, T.-L. Nguyen, T. Behrle, and J. P. Home, *Nat. Phys.* **18**, 296 (2022).
- [19] B. de Neeve, T.-L. Nguyen, A. Ferk, T. Behrle, F. Lancellotti, M. Simoni, S. Welte, and J. Home, *Modular variable laser cooling for efficient entropy extraction* (2024), arXiv:2408.16128 [quant-ph].
- [20] A. Eickbusch, V. Sivak, A. Z. Ding, S. S. Elder, S. R. Jha, J. Venkatraman, B. Royer, S. M. Girvin, R. J. Schoelkopf, and M. H. Devoret, *Nat. Phys.* **18**, 1464 (2022).
- [21] V. V. Sivak, A. Eickbusch, B. Royer, S. Singh, I. Tsioutsios, S. Ganjam, A. Miano, B. L. Brock, A. Z. Ding, L. Frunzio, S. M. Girvin, R. J. Schoelkopf, and M. H. Devoret, *Nature* **616**, 50 (2023).
- [22] K. Duivenvoorden, B. M. Terhal, and D. Weigand, *Phys. Rev. A* **95**, 012305 (2017).
- [23] K. Fukui, R. N. Alexander, and P. van Loock, *Phys. Rev. Res.* **3**, 033118 (2021).
- [24] F. Schmidt, D. Miller, and P. van Loock, *Phys. Rev. A* **109**, 042427 (2024).
- [25] M. Azari, P. Polakos, and K. P. Seshadreesan, in *ICC 2024 - IEEE International Conference on Communications* (IEEE, 2024) pp. 09–13.
- [26] K. Fukui, A. Tomita, and A. Okamoto, *Phys. Rev. Lett.* **119**, 180507 (2017).
- [27] A. L. Grimsmo and S. Puri, *PRX Quantum* **2**, 020101 (2021).
- [28] K. Noh, C. Chamberland, and F. G. S. L. Brandão, *PRX Quantum* **3**, 010315 (2022).
- [29] P. Dhara, L. Jiang, and S. Guha, arXiv 10.48550/arXiv.2406.04275 (2024), 2406.04275.
- [30] S. Konno, W. Asavanant, K. Fukui, A. Sakaguchi, F. Hanamura, P. Marek, R. Filip, J.-i. Yoshikawa, and A. Furusawa, *Phys. Rev. Res.* **3**, 043026 (2021).
- [31] M. H. Shaw, A. C. Doherty, and A. L. Grimsmo, arXiv 10.48550/arXiv.2403.02396 (2024), 2403.02396.
- [32] V. G. Matsos, C. H. Valahu, M. J. Millican, T. Navickas, X. C. Kolesnikow, M. J. Biercuk, and T. R. Tan, arXiv 10.48550/arXiv.2409.05455 (2024), 2409.05455.
- [33] M. Aghaee, A. A. Ramirez, Z. Alam, R. Ali, M. Andrzejczuk, A. Antipov, M. Astafev, A. Barzegar, B. Bauer, J. Becker, A. Bocharov, S. Boddapati, D. Bohn, J. Bommer, E. B. Hansen, L. Bourdet, A. Bousquet, S. Boutin, S. B. Markussen, J. C. E. Saldaña, L. Casparis, B. J. Chapman, S. Chatoor, C. Chua, P. Codd, W. Cole, P. Cooper, F. Corsetti, A. Cui, J. P. Dehollain, P. Dalpasso, M. de Moor, G. de Lange, A. Ekefjård, T. E. Dandachi, S. Fallahi, L. Galletti, G. Gardner, D. Govender, F. Griggio, R. Grigoryan, S. Grijalva, S. Gronin, J. Gukelberger, M. Hamdast, F. Hamze, M. H. Madsen, J. H. Nielsen, J. M. Nielsen, S. Heedt, Z. Heidarnia, J. H. Zamorano, S. Ho, L. Holgaard, J. Hornibrook, W. H. P. Nielsen, J. Indrapiromkul, H. Ingerslev, L. Ivancevic, J. Jhoja, J. Jones, K. V. Kalashnikov, R. Kallaher, F. Karimi, T. Karzig, E. King, M. E. Kloster, C. Knapp, D. Kocon, J. Koski, P. Kostamo, U. K. Bhaskar, M. Kumar, T. Laeven, T. Larsen, K. Lee, J. Lee, G. Leum, K. Li, T. Lindemann, M. Looij, J. Love, M. Lucas, R. Lutchyn, N. Madulid, A. Malmros, M. Manfra, D. Mantri, E. Martinez, M. Mattila, R. McNeil, R. V. Mishmash, G. Mohandas, C. Mollgaard, T. Morgan, G. Moussa, C. Nayak, B. Nijholt, M. Nystrom, E. O'Farrell, T. Ohki, K. Otani, B. P. Wütz, S. Pauka, K. Petersson, L. Petit, D. Pikulin, G. Prawiroatmodjo, F. Preiss, M. Rajpalke, C. Ranta, K. Rasmussen, D. Razmadze, O. Reentila, D. J. Reilly, Y. Ren, K. Reneris, A. R. Mei, R. Rouse, I. Sadovskyy, L. Sainiemi, I. Sanlorenzo, E. Schmidgall, C. Sfligoj, M. B. Shah, K. Simoes, S. Singh, S. Sinha, T. Soerensen, P. Sohr, T. Stankevic, L. Stek, E. Stuppard, H. Suominen, J. Suter, S. Teicher, N. Thyagarajah, R. Tholapi, M. Thomas, E. Toomey, J. Tracy, M. Turley, S. Upadhyay, I. Urban, K. Van Hoogdalem, D. J. Van Woerkom, D. V. Viazmitinov, D. Vogel, G. W. Winkler, J. Watson, A. Webster, J. Weston, A. W. Christensen, C. K. Yang, E. Yucelen, R. Zeisel, G. Zheng, and J. Zilke, *Interferometric Single-Shot Parity Measurement in an InAs-Al Hybrid Device* (2024), arXiv:2401.09549 [cond-mat] version: 1.
- [34] D. Niepce, J. Burnett, and J. Bylander, *Phys. Rev. Appl.* **11**, 044014 (2019).
- [35] These are related to the capacitor charge q and inductor flux φ through $\phi = 2\pi\varphi/\varphi_0$ and $n = q/2e$ with $\varphi_0 = h/2e$ the flux quantum. Due to the nonzero inductance, ϕ is decompactified.
- [36] We work in a gauge where the time-average of $\Phi(t)$ vanishes.
- [37] Here we consider doubly-degenerate square-lattice GKP states. Different encodings are briefly mentioned below, but are otherwise left for future studies. Also note that there is not a unique GKP encoding, even for square-encodings. Here we consider the natural one, however, which aligns with the 2π -periodicity of the Josephson junction.
- [38] G. Pantaleoni, B. Q. Baragiola, and N. C. Menicucci, *Phys. Rev. Lett.* **125**, 040501 (2020).
- [39] Since $[\sigma_i, \sigma_j] = 2\epsilon_{ijk}\sigma_k$, with ϵ_{ijk} the Levi-Civita tensor, the operators $\{\sigma_i\}$ form a valid qubit observable.
- [40] F. Nathan and M. S. Rudner, *Phys. Rev. B* **102**, 115109 (2020).
- [41] H.-P. Breuer and F. Petruccione, *The Theory of Open Quantum Systems* (Oxford University Press, Oxford, England, UK, 2002).
- [42] L. Guo, M. Marthaler, and G. Schön, *Phys. Rev. Lett.* **111**, 205303 (2013).
- [43] Y. Zhang, J. Gosner, S. M. Girvin, J. Ankerhold, and M. I. Dykman, *Phys. Rev. A* **96**, 052124 (2017).
- [44] F. Nathan, G. Refael, M. S. Rudner, and I. Martin, *Phys. Rev. Res.* **2**, 043411 (2020).
- [45] I.e., in the rotating frame generated by $U_r(t) = e^{-iH_r t}$, where $H_r = \frac{\hbar\Omega}{2}(\phi^2/2\pi\zeta - 2\pi\zeta\partial_\phi^2)$, where $\zeta \equiv \sqrt{L/C}/[h/4e^2]$.

- [46] K. Noh, V. V. Albert, and L. Jiang, *IEEE Transactions on Information Theory* **65**, 2563 (2019).
- [47] See, e.g., Refs. [63–68] for other applications of narrow-bandwidth baths to stabilize nontrivial driven-dissipative steady states.
- [48] P. Krantz, M. Kjaergaard, F. Yan, T. P. Orlando, S. Gustavsson, and W. D. Oliver, *Applied Physics Reviews* **6**, 021318 (2019).
- [49] While both inductive and capacitive coupling will lead to dissipative stabilization, for concreteness we consider capacitive coupling, as depicted in Fig. 1(a).
- [50] C. Gardiner and P. Zoller, *Quantum Noise* (Springer, Berlin, Germany, 2004).
- [51] G. Kiršanskas, M. Franckić, and A. Wacker, *Phys. Rev. B* **97**, 035432 (2018).
- [52] F. Nathan, *Topological Phenomena in Periodically Driven Systems*, Ph.D. thesis, University of Copenhagen (2018).
- [53] D. Davidović, *Quantum* **4**, 326 (2020).
- [54] F. Nathan and M. S. Rudner, *Phys. Rev. B* **109**, 205140 (2024).
- [55] A. Eckardt and E. Anisimovas, *New Journal of Physics* **17**, 093039 (2015), publisher: IOP Publishing.
- [56] I.e., to processes effectively involving net absorption of k drive photons and $z - 2k$ resonator photons in the lab frame for some $k \in \mathbb{Z}$.
- [57] J. Dalibard, Y. Castin, and K. Mølmer, *Physical Review Letters* **68**, 580 (1992), publisher: American Physical Society.
- [58] H. Carmichael, *Lecture Notes in Physics Monographs* **18**, 10.1007/978-3-540-47620-7 (1993), aDS Bibcode: 1993LNPM...18.....C.
- [59] The discretization is chosen adaptively for each parameter set to ensure that the region of phase space where the GKP states are confined, $|\phi\rangle$, $|2\pi\zeta n\rangle \lesssim \sqrt{8\pi\zeta\tilde{J}/\hbar\delta\omega}$, is well captured in the grid. Specifically, we choose a regularly spaced grid with spacing $\Delta\phi = 2\pi/[4\sqrt{2\tilde{J}/\pi\zeta\hbar\delta\omega}]$ and endpoints $\pm\phi_{\max}$, $\phi_{\max} = 2\pi \times [2\sqrt{2\zeta\tilde{E}_J/\pi\hbar\delta\omega}]$.
- [60] The gap limits the voltage amplitude V_0 , and thereby, the energy scale of all other parameters.
- [61] The generic high-temperature initial state is generated as an incoherent mixture of random states whose components in the discretized ϕ basis are given by $\psi_j = (a_j + ib_j)/\mathcal{N}$ with a_j, b_j randomly drawn from $[-1, 1]$, and \mathcal{N} a normalization prefactor.
- [62] Lifetimes τ_j , $j = x, y, z$ are obtained by a linear fit to the logarithm of the expectation values of the logical operators $\text{Tr}(\rho(t)\sigma_j)$ for the time-evolved density matrix.
- [63] K. I. Seetharam, C.-E. Bardyn, N. H. Lindner, M. S. Rudner, and G. Refael, *Physical Review X* **5**, 041050 (2015), publisher: American Physical Society.
- [64] T. Iadecola, T. Neupert, and C. Chamon, *Phys. Rev. B* **91**, 235133 (2015).
- [65] H. H. Yap, L. Zhou, J.-S. Wang, and J. Gong, *Phys. Rev. B* **96**, 165443 (2017).
- [66] I. Esin, M. S. Rudner, G. Refael, and N. H. Lindner, *Phys. Rev. B* **97**, 245401 (2018).
- [67] R. Zhang, F. Nathan, N. H. Lindner, and M. S. Rudner, *Phys. Rev. B* **110**, 075428 (2024).
- [68] H. Putterman, K. Noh, C. T. Hann, G. S. MacCabe, S. Aghaeimeibodi, R. N. Patel, M. Lee, W. M. Jones, H. Moradinejad, R. Rodriguez, N. Mahuli, J. Rose, J. C. Owens, H. Levine, E. Rosenfeld, P. Reinhold, L. Monceli, J. A. Alcid, N. Alidoust, P. Arrangoiz-Arriola, J. Barnett, P. Bienias, H. A. Carson, C. Chen, L. Chen, H. Chinkeziyan, E. M. Chisholm, M.-H. Chou, A. Clerk, A. Clifford, R. Cosmic, A. V. Curiel, E. Davis, L. DeLorenzo, J. M. D’Ewart, A. Diky, N. D’Souza, P. T. Dumitrescu, S. Eisenmann, E. Elkhoully, G. Evenbly, M. T. Fang, Y. Fang, M. J. Fling, W. Fon, G. Garcia, A. V. Gorshkov, J. A. Grant, M. J. Gray, S. Grimberg, A. L. Grimsmo, A. Haim, J. Hand, Y. He, M. Hernandez, D. Hover, J. S. C. Hung, M. Hunt, J. Iverson, I. Jarrige, J.-C. Jaskula, L. Jiang, M. Kalae, R. Karabalin, P. J. Karalekas, A. J. Keller, A. Khalajhedayati, A. Kubica, H. Lee, C. Leroux, S. Lieu, V. Ly, K. V. Madrigal, G. Marcaud, G. McCabe, C. Miles, A. Milsted, J. Minguzzi, A. Mishra, B. Mukherjee, M. Naghiloo, E. Oblepias, G. Ortuno, J. Pagdilao, N. Pancotti, A. Panduro, J. P. Paquette, M. Park, G. A. Peairs, D. Perello, E. C. Peterson, S. Ponte, J. Preskill, J. Qiao, G. Refael, R. Resnick, A. Retzker, O. A. Reyna, M. Runyan, C. A. Ryan, A. Sahnoud, E. Sanchez, R. Sanil, K. Sankar, Y. Sato, T. Scaffidi, S. Siavoshi, P. Sivaraiah, T. Skogland, C.-J. Su, L. J. Swenson, S. M. Teo, A. Tomada, G. Torlai, E. A. Wollack, Y. Ye, J. A. Zerrudo, K. Zhang, F. G. S. L. Brandão, M. H. Matheny, and O. Painter, *Hardware-efficient quantum error correction using concatenated bosonic qubits* (2024), arXiv:2409.13025 [quant-ph].
- [69] T. Kuwahara, T. Mori, and K. Saito, *Annals of Physics* **367**, 96 (2016).
- [70] The factor of 2 in \tilde{E}_J arises because the two terms in the sum in Eq. (A7) for $p = q = 1$ are identical.
- [71] F. Nathan, I. Martin, and G. Refael, *Physical Review B* **99**, 094311 (2019).
- [72] Here we ignored the Lamb shift that weakly renormalizes the Hamiltonian.
- [73] G. Floquet, *Annales scientifiques de l’École Normale Supérieure* **12**, 47 (1883).
- [74] T. Oka and S. Kitamura, *Annual Review of Condensed Matter Physics* **10**, 387 (2019), publisher: Annual Reviews.
- [75] T. Mori, *Annu. Rev. Condens. Matter Phys.* **14**, 35 (2023).
- [76] F. Nathan, *Topological Phenomena in Periodically Driven Systems (Ph.D. thesis)*, Ph.D. thesis, University of Copenhagen (2018).

Appendix A: Saddle-point approximation of effective Hamiltonian and generalized protocols

Here we show how the GKP Hamiltonian in Eq. (4) emerges as the effective Hamiltonian of the circuit, after making the rotating wave and saddle point—or stationary phase—approximations.

To recapitulate the problem, we consider an arbitrary time-periodic voltage signal $V(t) = V(t + T)$ with $T = 2\pi/\Omega$. To efficiently represent the dynamics of the system, we let $\Phi(t)$ denote the dimensionless phase induced by the oscillating voltage, defined such that

$$\partial_t \Phi(t) \equiv \frac{2e}{\hbar} V(t). \quad (\text{A1})$$

we pick the gauge where $\Phi(t)$ has zero mean, such that $\int_0^T dt \Phi(t) = 0$. The period of the oscillating voltage is near-commensurate with the resonator frequency ω : $\omega \approx \tilde{\Omega}$, where

$$\tilde{\Omega} \equiv \frac{p}{q} \Omega. \quad (\text{A2})$$

for incommensurate integers p and q . In terms of the phase, the Hamiltonian in the co-moving phase-space frame rotating with angular frequency $\tilde{\Omega}$, $\tilde{H}(t)$, is given by

$$\tilde{H}(t) = H_d - E_J \cos[\phi \cos \tilde{\Omega} t + 2\pi \zeta n \sin \tilde{\Omega} t - \Phi(t)] \quad (\text{A3})$$

where $H_d \equiv \frac{\hbar \delta f}{2} (\frac{\phi^2}{2\pi \zeta} + 2\pi \zeta n^2)$ denotes the detuning Hamiltonian with $\delta\omega = \omega - \tilde{\Omega}$ the frequency detuning from resonance. Note that the Hamiltonian $\tilde{H}(t)$ is time-periodic with *extended* period qT , $\tilde{H}(t) = \tilde{H}(t + qT)$. Our goal is to calculate the effective, or Floquet, Hamiltonian generated by $\tilde{H}(t)$, H_{eff} .

We first make the rotating wave approximation, which is valid when $\partial_t \Phi(t) = 2eV(t)/\hbar \gg E_J, \delta\omega$, and approximates H_{eff} by the time-average of $\tilde{H}(t)$ [69] over its full (extended) period: $H_{\text{eff}} \approx H_{\text{RWA}}$, where

$$H_{\text{RWA}} \equiv \int_0^{qT} \frac{dt}{qT} \tilde{H}(t). \quad (\text{A4})$$

In the following discussion, we focus on computing the time-average of the second term in Eq. (A3), since H_d is time-independent. For simplicity, we thus set $\delta\omega = 0$ below, resulting in H_d , unless noted otherwise.

We next write

$$H_{\text{RWA}} = - \int_0^{qT} \frac{dt}{2qT} E_J e^{-i[\phi \cos \tilde{\Omega} t - 2\pi \zeta n \sin \tilde{\Omega} t - \Phi(t)]} + h.c.. \quad (\text{A5})$$

To compute the integral above, we now use the saddle-point, or stationary phase approximation to compute the integral above. This approximation is valid when the characteristic scale of $\partial_t \Phi = 2eV(t)/\hbar$ is much larger than $\tilde{\Omega}$ —a condition which we have already satisfied when assuming the RWA to be valid. In this limit, the integral in Eq. (A4) only gets contributions

from the points $\{t_i\} \subset [0, qT)$ where $\tilde{\Phi}$ is stationary, $\partial_t \Phi(t_i) = 0$. Since $\partial_t \Phi(t) \propto V(t)$, the stationary points coincide with the nodes of the voltage signal, i.e., $\{t_i\} = \{t \in [0, qT) | V(t) = 0\}$. Using the stationary phase approximation we then obtain

$$H_{\text{RWA}} \approx - \sum_{i=1}^N \frac{E_J e^{-i[\phi \cos \tilde{\Omega} t_i - 2\pi \zeta n \sin \tilde{\Omega} t_i - \Phi(t_i) - \frac{\pi}{4} \mu_i]}}{2qT \sqrt{|\Phi''(t_i)|/2\pi}} + h.c.. \quad (\text{A6})$$

where $\mu_i \equiv \text{sgn}[\Phi''(t_i)]$. Using $\Phi'(t) = 2e/\hbar V(t)$, this leads to

$$H_{\text{RWA}} \approx - \sum_{i=1}^N \frac{E_J \cos[\phi \cos \tilde{\Omega} t_i - 2\pi \zeta n \sin \tilde{\Omega} t_i - \Phi(t_i) - \frac{\pi}{4} \mu_i]}{qT \sqrt{2e|V'(t_i)|/\hbar}}. \quad (\text{A7})$$

where the sum runs over all the nodes of $V(t)$ in the interval $[0, qT)$, t_1, \dots, t_N . This is the most general result.

We now consider two special cases in which the square-GKP and hexagonal-GKP stabilizer Hamiltonians emerge.

1. Emergence of square GKP stabilizer Hamiltonian

We can obtain the square GKP stabilizer Hamiltonian by driving at $\Omega \approx 2\omega$, i.e., $p = 1, q = 2$ with a waveform $V(t)$ that only consists of odd-harmonic sine waves,

$$V(t) = \sum_{n=0}^{\infty} c_n \sin([2n + 1]\Omega t) \quad (\text{A8})$$

for some coefficients $\{c_n\}$. This choice of waveform ensures that $V(t) = -V(-t)$ and $V(t) = -V(t + T/2)$, implying the waveform will have nodes at $t \in \frac{T}{4}\mathbb{Z}$. We moreover require that the harmonic coefficients $\{c_n\}$ are chosen such that these instances are the *only* nodes of $V(t)$. For instance, the waveform can be a pure sine wave: $c_0 = V_0, c_n = 0$ for $n \geq 1$ to obtain a pure sine wave; however, we allow more general waveforms allow for optimizing the protocol to improve the effective barrier height (thereby improving stability).

With the choice above, the nodes of the voltage signal within the extended period $2T$ occur at the four instances $\{t_i\} = \{0, \frac{1}{2}T, T, \frac{3}{2}T\}$, corresponding to $\{\tilde{\Omega} t_i\} = \{0, \frac{\pi}{2}, \pi, \frac{3\pi}{2}\}$. Without loss of generality, we moreover assume $V'(0) \geq 0$ —this can be ensured with appropriate choice of time-origin. As a result $\mu_i = (-1)^{i+1}$, while $|V'(t_i)| = |V'(0)|$ for $i = 1, \dots, 4$. Finally, $\Phi(t_i)$ is given by $-(-1)^i \Phi(0)$. With the gauge choice that $\Phi(t)$ has zero time-average, $\Phi(0)$ is uniquely defined, and given by $-\Phi_0$, where

$$\Phi_0 \equiv \int_0^{T/4} dt \frac{2eV(t)}{\hbar}. \quad (\text{A9})$$

Inserting these results in Eq. (A7), using $q = 2$, and explicitly writing out all 4 terms, we obtain

$$H_{\text{RWA}} \approx \frac{-E_J}{2T\sqrt{2e|V'(0)|/\hbar}} \left(\cos\left[\phi + \Phi_0 - \frac{\pi}{4}\right] + \cos\left[-\phi + \Phi_0 - \frac{\pi}{4}\right] + \cos\left[2\pi\zeta n - \Phi_0 + \frac{\pi}{4}\right] + \cos\left[-2\pi\zeta n - \Phi_0 + \frac{\pi}{4}\right] \right) \quad (\text{A10})$$

Using $\cos(a+b) = \cos(a)\cos(b) + \sin(a)\sin(b)$, we obtain

$$H_{\text{RWA}} \approx -\frac{E_J \cos(\Phi_0 - \pi/4)}{T\sqrt{2e|V'(0)|/\hbar}} (\cos\phi + \cos 2\pi\zeta n) \quad (\text{A11})$$

with $\zeta \in \mathbb{Z}$ we thus recover the stabilizer Hamiltonian for a square-lattice GKP qubit with ζ -fold degeneracy. In the presence of nonzero detuning, an extra term H_d is added to H_{RWA} . This is the result we quoted in the main text.

2. Emergence of hexagonal GKP stabilizer Hamiltonian

We now show how the hexagonal GKP code can be generated by a odd-harmonic sine drive similarly to the square-lattice Hamiltonian [Eq. (A8)] (or a higher-order featuring odd sines), but with $\Omega \approx 3\omega$ or $\Omega \approx 3\omega/2$ —i.e., with $q = 3$ and $p = 1, 2$. For simplicity we focus on the case $\Omega \approx 3\omega$ ($q = 3, p = 1$). In this case, the waveform $V(t)$ has 6 nodes within the extended period $3T$, namely at $t = n/6$ for $n = 0, 1, 2, 3, 4, 5$, corresponding to $\tilde{\Omega}t = 2\pi z/6$.

Explicitly summing over all these 6 nodes in Eq. (A7), we obtain

$$H_{\text{RWA}} \approx -\frac{E_J}{3T\sqrt{2e|V'(0)|/\hbar}} \sum_{z=1}^3 [\cos(\phi c_z - 2\pi\zeta n s_z + (-1)^z[\Phi_0 + \pi/4]) + \cos(-\phi c_z + 2\pi\zeta n s_z - (-1)^z[\Phi_0 - \pi/4])] \quad (\text{A12})$$

where

$$c_z = \cos\left(\frac{2\pi z}{6}\right) \quad s_z = \sin\left(\frac{2\pi z}{6}\right). \quad (\text{A13})$$

Here we paired up the terms i and $i+3$ (for $i = 1, 2, 3$) from the sum in Eq. (A7) to form the summand above. Using that $\cos(x) = \cos(-x)$, we see that the two terms in each summand are identical, leading to

$$H_{\text{RWA}} \approx -\frac{2E_J}{3T\sqrt{2e|V'(0)|/\hbar}} \sum_{z=1}^3 \cos(\phi c_z - 2\pi\zeta n s_z + (-1)^z[\Phi_0 - \pi/4]) \quad (\text{A14})$$

This gives

$$H_{\text{RWA}} \approx -\frac{2E_J}{3T\sqrt{2e|V'(0)|/\hbar}} \sum_{z=1}^3 \cos(c_z \phi - 2\pi s_z \zeta n - (-1)^z[\Phi_0 + \pi/4]) \quad (\text{A15})$$

When $\zeta = \frac{k}{\sin 2\pi/3} = \frac{2k}{\sqrt{3}}$ for integer k , all 3 terms in the sum above commute, and H_{RWA} becomes a stabilizer Hamiltonian for the Hexagonal GKP code, protecting a k -dimensional qudit. In particular, if we ensure that $\Phi_0 = \pi/4 + 2\pi z$ for integer z , we have

$$H_{\text{RWA}} \approx -\frac{2E_J}{3T\sqrt{2e|V'(0)|/\hbar}} \sum_{z=1}^3 \cos\left(c_z \phi - \frac{4\pi k}{\sqrt{3}} n s_z\right) \quad (\text{A16})$$

which is the hexagonal GKP stabilizer Hamiltonian that protects a k -dimensional qudit in its low-energy subspace.

We verify that the hexagonal states indeed emerge by calculating numerically the Wigner function of the steady-state density matrix after initialization from a random mixed state when driving close to thrice the resonance frequency with suitable system parameters, see Fig. 6 for the result.

Appendix B: S gate protocol

Here we provide further details on how a protected S gate might be generated with the circuit with the square-

GKP encoding, using the phase-revival mechanism de-

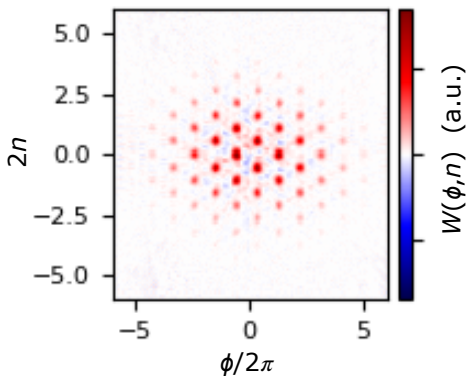


FIG. 6. Wigner function of a steady-state density matrix for driving at $\Omega \approx 3 \times 2\pi f_0$ after time-evolution of $t = 2000f_0^{-1}$ starting from a random mixed state. This density matrix corresponds to a mixed state in the hexagonal GKP encoding. System parameters: Josephson energy $E_J = 2.25f_0$, dimensionless impedance $\zeta = 4/\sqrt{3}$, cosine drive $\phi(t) = A \cos \Omega t$ with $A = 40.5\pi$ and $\Omega = 2\pi(3f_0 - \delta f)$ with detuning $\delta f = 0.004f_0$, resistor temperature $T_E = 0.016f_0$, low-pass filter with bandwidth $\Lambda_B = 0.07f_0$, and dimensionless coupling strength $\kappa = 10^6$.

scribed in Ref. [7]. We use the odd-harmonic sine waveform used in the main text and discussed in Sec. E. To implement an S gate, we first shift the GKP lattice by $\phi \rightarrow \phi + \pi$ by adiabatically increasing the amplitude of an extra tone with angular frequency $\tilde{\Omega}$, V_s , from zero to $\pi\hbar\tilde{\Omega}/2e$. This results in a shift of the phase signal $\Phi(t)$ by $\Delta\Phi(t) = \frac{2eV_s}{\hbar\tilde{\Omega}} \cos\tilde{\Omega}t$, resulting in the effective Hamiltonian being given by

$$H_{\text{RWA}} \approx \frac{-E_J \cos(\Phi_0 - \pi/4)}{T\sqrt{2e|V'(0)|/\hbar}} [\cos(\phi - 2eV_s/\hbar\Omega) + \cos 4\pi n]. \quad (\text{B1})$$

This result follows from direct insertion of the new phase signal $\Phi(t)$ into Eq. (A7) under the assumption that V_s is only weakly affecting $V'(t)$ at the nodes of the voltage oscillation (a simplifying, but not essential assumption). Under the adiabatic ramp of V_s , the wells in the $\cos\phi$ potential of the effective Hamiltonian, H_{RWA} get shifted adiabatically from $2\pi\mathbb{Z} + \pi$ to $2\pi\mathbb{Z} + \pi + 2eV_s/\hbar\Omega$, until they are located at $\phi \in 2\pi\mathbb{Z}$.

After the adiabatic shift of the well centers, we abruptly change the main driving tone to a new tone with frequency $f' \approx f/2$, i.e., with approximately doubled period $T' \approx 2T$. The amplitude of the period-doubled driving pulse should be adjusted so that $\Phi_0 = -3\pi/4$ and ideally have the same nodal slope $V'(0)$ as the original driving pulse. After the period-doubling of the signal, there are just two nodes of $V(t)$ in the extended period (which now coincides with T), namely $t = 0$ and $t = T/2$. Using the formula in Eq. (A7), the approximate effective Hamiltonian of the system becomes

$$H_{\text{eff}} \approx -\tilde{E}_J \cos \phi + \frac{\hbar\delta f'}{2} \left(\frac{\phi^2}{4\pi} + 4\pi n^2 \right) \quad (\text{B2})$$

where $\delta f' \equiv f' - f$ is the detuning of the frequency of the period-doubled signal from f_0 . To arrive at the above result, we used $\Phi_0 = -3\pi/4$, $\tilde{E}_J = \frac{2E_J}{T\sqrt{2e|V'(0)|/\hbar}}$ [70]. Note that the detuning of the period-doubled pulse, $\delta f'$ can be distinct from the usual driving pulse, and indeed will play crucial role.

The effective Hamiltonian above describes a free particle with mass $1/8\pi^2\delta f'$ in a potential consisting of a parabola with curvature $\delta f'/2$ and a cosine potential of amplitude \tilde{E}_J . When $\tilde{E}_J \gg \hbar\delta f'$, the low-energy eigenstates of H_{eff} are confined within the individual wells; the spectra and eigenstates of each well are near-identical, except for an overall energy shift for each well, which for the well at $\phi = 2\pi k$ is given by $\frac{\pi\hbar\delta f'}{2}k^2$. A GKP state with expectation value $\langle\sigma_z\rangle = \pm 1$ is a coherent superposition of states with support in even (+) or odd (−) wells, whose constrictions to individual well are near-identical. Under evolution by H_{eff} above for a duration of $\Delta t = 1/2\pi\delta f'$, the component of the state in well k will have acquired a phase factor $e^{-i\frac{\pi}{2}k^2}$ relative to the component in well zero. Since $k^2 \bmod 4 = 0$ for even k and $k^2 \bmod 4 = 1$ for odd k , components in odd wells will thus have acquired a phase factor i relative to their counterparts in even wells after the time span Δt . This is equivalent to the action of an S gate. Reverting to the original driving tone after this time-span will again activate the stabilizer term $\cos(4\pi n)$ in the effective Hamiltonian, stabilizing the state after the gate. A similar mechanism is described in Ref. [7], which shows that such a gate is expected to be exponentially robust against control noise.

Appendix C: Readout protocol

Here we provide additional details on the operating principle of the readout protocol.

To recap, the readout is achieved by (1) connecting a secondary, weak Josephson junction J' at a new circuit node located halfway along the inductor and (2) applying a separate voltage tone $V_R(t)$ across J' with a quadrupled period (frequency $f_R = f/4$). The circuit diagram is shown in Fig. 5(a) in the main text. The new node is henceforth referred to as the readout node. In the following, we show that the time-averaged supercurrent \bar{I} across J' is positive for even and negative for odd wells, thereby distinguishing the two logical states.

To establish the results above, we first seek to express the mean supercurrent in the secondary junction in terms of the resonator state evolution $\rho(t)$. We assume that the capacitance at the readout node is small, and that the secondary junction inductance $L_{J'} = E_{J'}/\varphi_0^2$ remains small relative to that of the main inductor, L , such that (a) the phase at the readout node remains relatively unperturbed by the secondary Josephson junction, and (b) the spectrum of modes in the resonator remains relatively unperturbed by the secondary Josephson junction, allowing all but the fundamental mode to be frozen out of the

dynamics. In this case, the phase at the readout node is given by $\phi/2$, due to its location halfway along the inductor. The supercurrent through the secondary Josephson junction will then be given by

$$I(t) = \frac{2eE_{J'}}{\hbar} \sin\left[\frac{\phi}{2} - \Phi_{\text{R}}(t)\right] \quad (\text{C1})$$

with $\Phi_{\text{R}}(t)$ the phase-oscillation induced by $V_{\text{R}}(t)$.

Having established the expression for the supercurrent operator of the second node, we can find \bar{I} via

$$\bar{I} = \lim_{N \rightarrow \infty} \frac{1}{N} \sum_n \bar{I}_n \quad (\text{C2})$$

where \bar{I}_n denotes the mean supercurrent through the junction over the n th period of the bias oscillation $V_{\text{R}}(t)$:

$$\bar{I}_n \equiv \int_{4nT}^{(n+1)4T} \frac{dt}{4T} \text{Tr}[\rho(t)I(t)]. \quad (\text{C3})$$

where $V_{\text{R}}(t)$ has periodicity $4T$, with $T = 1/f$ the period of the drive.

Using the expression in Eq. (C1), we find

$$\bar{I}_n = \frac{2eE_{J'}}{\hbar} \int_{4nT}^{4(n+1)T} \frac{dt}{4T} \Im \text{Tr}[\rho(t)e^{-i\phi/2}] e^{-i\Phi_{\text{R}}(t)} \quad (\text{C4})$$

In the limit of rapid phase oscillation, $\partial_t \Phi_{\text{R}}(t) \gg \partial_t \text{Tr}[\rho(t)e^{-i\phi/2}]$, we can approximate the integral above using the stationary phase approximation, as we did to obtain the effective Hamiltonian in Sec. A. Assuming an odd-harmonic sine waveform, $\Phi_{\text{R}}(t)$ has stationary points at the voltage nodes, $t_0 = 4nT$ and $t_1 = 4(n+1/2)T$. The stationary-phase approximation then yields

$$\bar{I}_n \approx \frac{eE_{J'}}{2T\hbar} \Im \sum_{k=0}^1 \frac{e^{-i\Phi_{\text{R}}(t_k) - i\frac{\pi}{4}\mu_k}}{\sqrt{|\Phi_{\text{R}}''(t_k)|/2\pi}} \text{Tr}[\rho(t_k)e^{-i\phi/2}] \quad (\text{C5})$$

with $\mu_k = \text{sgn}(\Phi_{\text{R}}''(t_k))$. For odd-harmonic sine waveform, we have $\Phi_{\text{R}}(t_k) = (-1)^k \Phi_{\text{R},0}$, and $\mu_k = (-1)^k$ for $k = 0, 1$, with $\Phi_{\text{R},0}$ the phase oscillation amplitude induced by $V_{\text{R}}(t)$. Using these results along with $\Phi_{\text{R}}''(t) = 2e/\hbar V_{\text{R}}'(t)$, we find

$$\bar{I}_n \approx \frac{eE_{J'}}{2T\hbar\sqrt{\varphi_0|V_{\text{R}}'(0)|}} \Im \sum_{i=0}^1 \text{Tr}[\rho(t_i)e^{-i\phi/2}] e^{-i(-1)^i[\Phi_{\text{R},0} - \frac{\pi}{4}]} \quad (\text{C6})$$

Neglecting the effect of the weak Josephson junction J' , the time evolution of the resonator density matrix is given by

$$\rho(t) \approx R_{\hat{\Omega}t}^\dagger e^{-iH_{\text{eff}}t} \rho(0) e^{iH_{\text{eff}}t} R_{\hat{\Omega}t} \quad (\text{C7})$$

where H_{eff} is the effective time-averaged Hamiltonian as obtained in Eq. (4) and R_θ rotates phase space by an angle θ , and $\hat{\Omega} = \pi/T$ is the angular frequency of the rotating frame. Since the strength of the GKP potential

by assumption is much weaker than $2hf_0$, $\tilde{E}_J \ll 2hf_0$, the evolution in the rotating frame is near-stationary over a single period, $e^{-iH_{\text{eff}}T} \approx 1$, implying

$$\rho(2(2n+1)T) \approx \rho(4nT). \quad (\text{C8})$$

Hence

$$\bar{I}_n \approx \frac{eE_{J'}}{2T\hbar} \Im \sum_{k=0}^1 \frac{e^{-i(-1)^k[\Phi_{\text{R},0} - \frac{\pi}{4}]} \text{Tr}[\rho(4nT)e^{-i\phi/2}]}{\sqrt{2e|V_{\text{R}}'(0)|/\hbar}} \quad (\text{C9})$$

Evaluating the sum, we find

$$\bar{I}_n \approx I_0 \text{Tr}[\rho(4nT) \sin(\phi/2)] \quad (\text{C10})$$

where

$$I_0 \equiv \frac{eE_{J'} \cos(\Phi_0 - \frac{\pi}{4})}{T\hbar\sqrt{\varphi_0|V_{\text{R}}'(0)|}} \quad (\text{C11})$$

Thus, the mean supercurrent is given by

$$\bar{I} \approx \bar{I}_0 \lim_{N \rightarrow \infty} \sum_{n=1}^N \frac{1}{N} \text{Tr}[\rho(4nT) \sin(\phi/2)] \quad (\text{C12})$$

We now consider the possible measurement outcomes: eigenstates with support even wells—i.e., $\phi \in 4\pi\mathbb{Z} + \pi$ (such as $|0\rangle$)—will result in $\bar{I} \approx \bar{I}_0$, while eigenstates with support in odd wells (such as $|1\rangle$)—i.e., $\phi \in 4\pi\mathbb{Z} - \pi$ —will result in $-\bar{I} \approx -\bar{I}_0$; the logical state is thus measured by the protocol.

The readout protocol can be used for initialization: initializing the system in a random state, the stabilization protocol will take the system into the code subspace. Subsequently measuring the state with the protocol above will collapse it into a logical $|0\rangle$ or $|1\rangle$ state, depending on the measurement outcome.

Appendix D: Modeling dissipative dynamics

In this section, we describe how the driven-dissipative dynamics of the circuit may be modeled with the universal Lindblad equation from Ref. [40, 71], and how this dynamics results in the time-independent effective master equation in Eq. (5) of the main text. We also discuss the consequences of extrinsic noise for the dynamics.

To recap, the circuit can be analyzed as a periodically driven system with time-dependent Hamiltonian

$$H(t) = \frac{\hbar f_0}{2} \left(\frac{\phi^2}{2\pi\zeta} + 2\pi\zeta n^2 \right) - E_J \cos(\phi + \Phi(t)), \quad (\text{D1})$$

We couple the circuit to an external bath via

$$H_{\text{RC}} = \frac{2enQ_{\text{B}}(t)}{C_{\text{B}}}, \quad (\text{D2})$$

where $Q_{\text{B}}(t)$ denotes the fluctuating charge on the resistor-side of the coupler, and C_{B} the capacitance of

the coupler. We model $Q_B(t)$ as a quantum noise variable with equilibrium power spectral density,

$$J(E) \equiv \frac{4e^2}{2\pi C_B^2} \int dt \langle Q_B(t) Q_B(0) \rangle e^{iEt/\hbar}, \quad (\text{D3})$$

For now, we let the power spectral density be arbitrary, and restrict to filtered baths below.

In the Markovian regime, where the characteristic rate of system-bath coupling is much weaker than the characteristic inverse correlation time of the bath, Ref. [40] shows that the time-evolution of the reduced density matrix of the system evolves according to [72]

$$\partial_t \rho(t) = -i[H(t), \rho(t)] + L(t)\rho(t)L^\dagger(t) - \frac{1}{2}\{L^\dagger(t)L(t), \rho(t)\} \quad (\text{D4})$$

where the time-dependent jump operator $L(t)$ is given by

$$L(t) = \int ds g(t-s) U(t,s) n U(s,t) \quad (\text{D5})$$

where $U(t,s) \equiv U(t)U^\dagger(s)$ is the evolution operator from time t to time s , and

$$g(t) = \int d\omega e^{-i\omega t} \sqrt{2\pi J(\hbar\omega)} \quad (\text{D6})$$

denotes the *jump correlator*.

a. Floquet preliminaries

Being a Floquet problem, the time-evolution can be parameterized efficiently using a complete orthonormal basis of time-periodic *Floquet states*, $\{|\psi_n(t)\rangle = |\psi_n(t+T)\rangle\}$

and associated *quasienergies* $\{\varepsilon_n\}$. Specifically, the time-evolution generated by $H(t)$ of any state $|\Psi(t)\rangle$, can be expressed as $|\Psi(t)\rangle = \sum_n c_n e^{-i\varepsilon_n t} |\psi_n(t)\rangle$ [73, 74]; equivalently, the time-evolution operator of the system, $U(t)$, can be parameterized via

$$U(t) = \mathcal{M}(t) e^{-iH_{\text{eff}} t}, \quad (\text{D7})$$

where $\mathcal{M}(t) = \sum_n |\psi_n(t)\rangle \langle \psi_n|$ denotes the unitary *micromotion operator* and $H_{\text{eff}} = \sum_n \varepsilon_n |\psi_n\rangle \langle \psi_n|$ denotes the *effective Hamiltonian* of the system, described in the main text. Note that $\mathcal{M}(t) = \mathcal{M}(t + \tilde{T})$ and $\mathcal{M}(0) = \mathcal{M}(n\tilde{T}) = 1$, for $n \in \mathbb{Z}$.

Importantly, there is a gauge freedom in choosing the quasienergies—in particular limits, such as high or low frequency limits, some choices are better than others however—in these two limits, the quasienergies match up with the eigenvalues of the time-averaged Hamiltonian and the time-averaged energies of the instantaneous Hamiltonian (plus geometric phases), respectively. We choose to view it as a period-doubled problem, using $\tilde{T} = 2T$ as the extended period. In this case it is possible to choose the quasienergy zone such that $H_{\text{eff}} \approx H_{\text{RWA}}$ and $\mathcal{M}(t) \approx R_{\tilde{\Omega}t}$, where $R_\theta = \exp\left[-i\frac{\theta}{2}\left(\frac{\phi^2}{2\pi\zeta} + 2\pi\zeta n^2\right)\right]$ generates a rotation of phase space by angle θ [42–44]; the convergence can be formally proven in the high-frequency limit [55].

1. Dissipative dynamics in Floquet frame

Having laid out the preliminaries of Floquet theory, we now formulate the problem in the *Floquet frame* [75], i.e., the frame comoving with $\mathcal{M}(t)$. Specifically, we consider the evolution of the density matrix $\rho'(t) = \mathcal{M}(t)\rho(t)\mathcal{M}^\dagger(t)$, which coincides with $\rho(t)$ for $t \in \mathbb{Z}T$. In this frame, the equation of motion reads

$$\partial_t \rho'(t) = -i[H_{\text{eff}}, \rho'(t)] + L'(t)\rho'(t)L'^\dagger(t) - \frac{1}{2}\{L'^\dagger(t)L'(t), \rho'(t)\}. \quad (\text{D8})$$

where $L'(t) \equiv \mathcal{M}^\dagger(t)L(t)\mathcal{M}(t)$. The jump operator is then given by [40, 71, 76]

$$L'(t) = \sum_z e^{-i\tilde{\Omega}zt} L_z \quad (\text{D9})$$

where

$$L_z = \sum_{ab} \sqrt{2\pi J(\varepsilon_a - \varepsilon_b + z\tilde{\Omega})} |\psi_a\rangle \langle \psi_a | \bar{n}_z |\psi_b\rangle \langle \psi_b|, \quad \text{and} \quad \bar{n}_z \equiv \frac{1}{T} \int_0^T dt \langle \mathcal{M}^\dagger(t) n \mathcal{M}(t) e^{iz\Omega t} \rangle. \quad (\text{D10})$$

While Eq. (D8) in principle can be solved, we can make a further simplifying rotating wave approximation that cancels out the cross terms between from coefficients L_z and $L_{z'}$ for $z \neq z'$ that arises by insertion of Eq. (D9) into Eq. (D8). As a first step, we expand Eq. (D8) in terms of the coefficients $\{L_z\}$, obtaining

$$\partial_t \rho'(t) = -i[H_{\text{eff}}, \rho'(t)] + \sum_{z_i = -\infty}^{\infty} e^{-i(z_1 - z_2)\tilde{\Omega}t} \left[L_{z_1} \rho'(t) L_{z_2}^\dagger - \frac{1}{2} \{L_{z_2}^\dagger L_{z_1}, \rho'(t)\} \right] \quad (\text{D11})$$

Next, we note that states in the code-subspace coincide with the low-lying eigenstates of the GKP Hamilto-

nian, and hence have quasienergies in $[-\tilde{E}_J, \tilde{E}_J]$. Mov-

ing away from the code-subspace towards the high-energy limit, the energy spectrum gradually turns into an evenly spaced spectrum of harmonic oscillator eigenstates confined near LC photon number $n_{\text{ph}} = E/\delta\omega$ for energy E . At the same time, the eigenstates of the GKP Hamiltonian (having energy of order $\lesssim \tilde{E}_J$) are confined near photon number $n_{\text{ph}} \sim \tilde{E}_J/\delta\omega$. When $\Omega \gg \tilde{E}_J$, the phase space (photon number) support of states in the code subspace and states with $E > \Omega$ is thus highly disjoint, and $X_{ab;z} \equiv \frac{1}{T} \int_0^T dt \langle \psi_a(t) | n | \psi_b(t) \rangle e^{izz\Omega t} = 0$ for these states. As long as $\rho(t)$ maintains its support in the code subspace, we can therefore set $n_{ab;z} = 0$ up to exponentially small corrections all for states where $|\varepsilon_a - \varepsilon_b| \gtrsim \tilde{\Omega}$. In the limit $\tilde{\Omega} \gg \tilde{E}_J$, cross-terms in Eq. (D11), where $z_1 \neq z_2$, are thus highly oscillatory relative to all other frequency scales in the equation, and hence can be eliminated via a rotating wave approximation. This results in the *time-independent* master equation in [Eq. (5)] of the main text,

$$\partial_t \rho' = -i[H_{\text{eff}}, \rho'] + \sum_{z=-\infty}^{\infty} \left[L_z \rho L_z^\dagger - \frac{1}{2} \{L_z^\dagger L_z, \rho'\} \right], \quad (\text{D12})$$

as we sought to establish.

Appendix E: Capped voltage tone

To reduce the maximal voltage across the Josephson junction during the drive, we cap the voltage by considering a drive of the form

$$V(t) = V_0 \sum_{n=0}^N a_n \sin((2n+1)\Omega t) \quad (\text{E1})$$

where the coefficients a_n are chosen such that the $2n$ 'th derivative vanishes at $\Omega t = \pi/2$ while the slope at the voltage nodes $dV/dt(\Omega t = 0) = V_0\Omega$ is kept equal to the slope of a sinusoidal drive.

For the voltage pulse used in the main text, we used $N = 6$. The coefficients are explicitly

$$\begin{aligned} a_0 &= 429/1024, & a_1 &= 143/4096 \\ a_2 &= 143/20480, & a_3 &= 143/100352 \\ a_4 &= 13/55296, & a_5 &= 13/495616 \\ a_6 &= 1/692224 \end{aligned}$$

so that $\max V(t) = \frac{1024}{3003} V_0 \approx 0.340992 V_0$. The voltage cap is chosen by comparing lifetime calculations with different caps, and then choosing the minimal voltage cap where the lifetime is not significantly reduced.

Appendix F: Operation with a low-pass filter

A possible challenge of the band-pass filter discussed in the main text is to achieve a sharp cutoff of the filter

f_0	δf	E_J/h	$\Gamma_{\tilde{a}}/2\pi$	κ	Λ_B	T_E	V_0
17 GHz	36 MHz	54 GHz	17 kHz	200	1.2 GHz	10 mK	3.0 mV
-	$.0021f_0$	$3.2f_0$	$10^{-6}f_0$	200	$.07f_0$	$.012f_0$	$21f_0$

TABLE II. **Parameters probed for low-pass filter operation.** *Row 1:* Default parameters for simulations operating with the low-pass filter whose numerical results are shown in Fig. 7 and Fig. 8. *Row 2:* Parameter values in terms of the resonator frequency, f_0 , in units where $h = e = k_B = 1$.

spectral function at $E = \hbar\Omega$ so that photon-emission-assisted excitations in the GKP subspace are suppressed. Here we discuss how this challenge can be avoided by instead operating the system with a low-pass filter.

The low-pass filter approach can be implemented with a bath filter whose spectral density $S(E)$ has support constrained to $|E| \leq \hbar\tilde{\Omega}/2$ (but not necessarily with sharp edges). In this case, only L_0 is nonzero in Eq. (5) [identical to Eq. (D12)], where

$$L_0 = \sum_{ab} \sqrt{2\pi J(\varepsilon_a - \varepsilon_b)} |\psi_a\rangle \langle \psi_a | n_0 | \psi_b\rangle \langle \psi_b|. \quad (\text{F1})$$

Hence the evolution is equivalent to that of a non-driven system with Hamiltonian H_{eff} connected to a thermal bath at temperature T_E and spectral density $S(E)$, through the system-bath coupling \tilde{n}_0 . Hence the system thermalizes with respect to the effective Hamiltonian and the equilibrium temperature. As a result, the protocol will work when $T \ll E_J$.

The low-pass filter approach does require a much smaller filter temperature $k_B T_E \ll \tilde{E}_J$. In order for the error correction to set on at a sufficiently large filter temperature, one needs to increase the resonator frequency. However, increasing the resonator and drive frequency limits the maximally achievable phase driving amplitude $\Phi_0 \ll \frac{2\Delta_0}{\alpha\hbar\Omega}$ where Δ_0 is the superconducting gap at the Josephson junction, and $\alpha \approx 0.340992$ is the factor from the capped voltage waveform [Sec. E]. These two constraints put a relatively tight bound on the device parameters, where we provided an example parameter set fine-tuned for NbN Josephson junctions in Table II.

Furthermore, the low-pass filter couples to the resonator charge directly and allows absorption of energy without additional resonator photons. These processes have low probability, because the corresponding matrix elements (D10) in the jump operator almost average to zero over one period – the only non-zero contribution comes from the micromotion. As a consequence, the jump operator connecting to the filtered bath also have a large logical error probability.

In Figs. 7,8, we present numerical results demonstrating the operation with a low-pass filter. The default parameters for this set of numerical results are shown in Table II. The parameter set is chosen to be reasonable for realization with NbN superconductors. Importantly, we choose a larger resonator frequency $f_0 = 17$ GHz to have a higher temperature window available. The max-

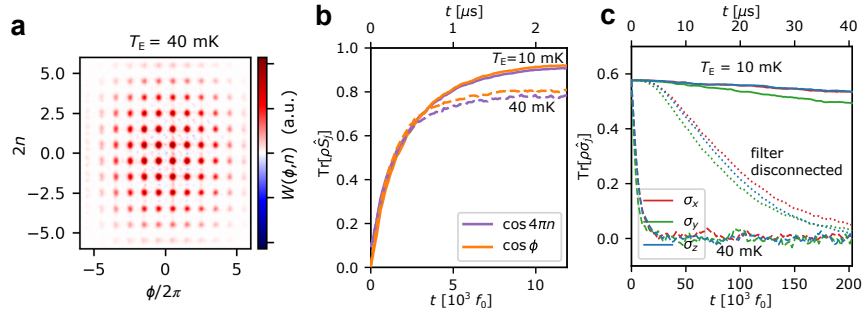


FIG. 7. **Stabilization of GKP states with low-pass filter approach.** (a) Final-state Wigner function of the density matrix and (b) GKP stabilizers for an evolution through 4000 periods of the voltage tone, starting from a high-temperature mixed state for filter temperature $T_E = 10$ mK (solid lines) and $T_E = 40$ mK (dashed). (b) Logical information stored in a GKP state initialized in an equal superposition of σ_x , σ_y , and σ_z expectation values with filter temperature $T_E = 10$ mK (solid lines) and $T_E = 40$ mK (dashed) and without coupling to a filter (dotted), demonstrating a lifetime enhancement by a factor ≈ 20 at 10 mK.

imal amplitude of the voltage drive V_{\max} is constrained by the superconducting gap $\Delta \approx 3\text{meV}$ for NbN Josephson junctions (voltages above the gap would lead to quasiparticle tunneling, that we expect induce logical errors). Achievable filter temperature (favoring a larger resonance frequency f_0) and maximal voltage (favoring a smaller f_0) are limiting the device performance for the low-pass filter operation. Therefore, we here use a smaller driving amplitude $\Phi_0/2\pi = 9.125$ and larger detuning $\delta f = 0.0021 f_0$ compared to the band-pass filter operation discussed in the main text.

We demonstrate initialization and stabilization of GKP states in Fig. 7 for two resistor temperatures that we expect are achievable, 10 mK and 40 mK. Figs. 7(a,b) show the resulting Wigner function of the final state at 40mK (a) and evolution of GKP stabilizers at 10mK and 40mK (b), respectively. Here, for both 10mK and 40mK, the system relaxes to a GKP state within $2000f_0^{-1} \approx 120$ ns. The evolution of logical operators [7(c)] demonstrates a significant improvement of the qubit lifetime at temperature $T_E = 10$ mK. At $T_E = 40$ mK, lifetime is reduced due to thermal activation across the barriers of H_{eff} even though the GKP states remain stabilized. In comparison to the operation with the band-pass filter in the main text, the low-pass filter exhibits lower logical lifetimes when thermal activation over the barrier is rel-

evant. We expect this to be because the jump operators for the filtered bath have a larger logical error rate for the low-pass filter as their matrix elements are dominated by the micromotion with large non-local coupling.

Numerical results for the lifetimes of logical information as a function of system parameters are presented in Fig. 8. Most results are qualitatively similar to the results from the band-pass filter, except for an overall smaller lifetime due to the larger detuning δf and smaller driving amplitude Φ_0 used here.

The main qualitative differences compared to the band-pass filter operation discussed in the main text are: First, (i), the coupling κ to the filtered bath needs to be much stronger [Fig. 8(a)]; this is because the $z = 0$ matrix elements for the phase-space-local capacitive coupling to the filtered bath are proportional to only small corrections arising from the micromotion. Second, (ii), the dependence on the filter temperature [Fig. 8(b)]: For the low-pass filter, thermal activation over the barrier is limited by the GKP barrier height \tilde{E}_J [as defined around Eq. (4) in the main text] so that temperature needs to be small compared to this energy scale. Finally, (iii), the low-pass filter operation has a larger tolerance towards deviations in the impedance [Fig. 8(f)] than the band-pass filter.

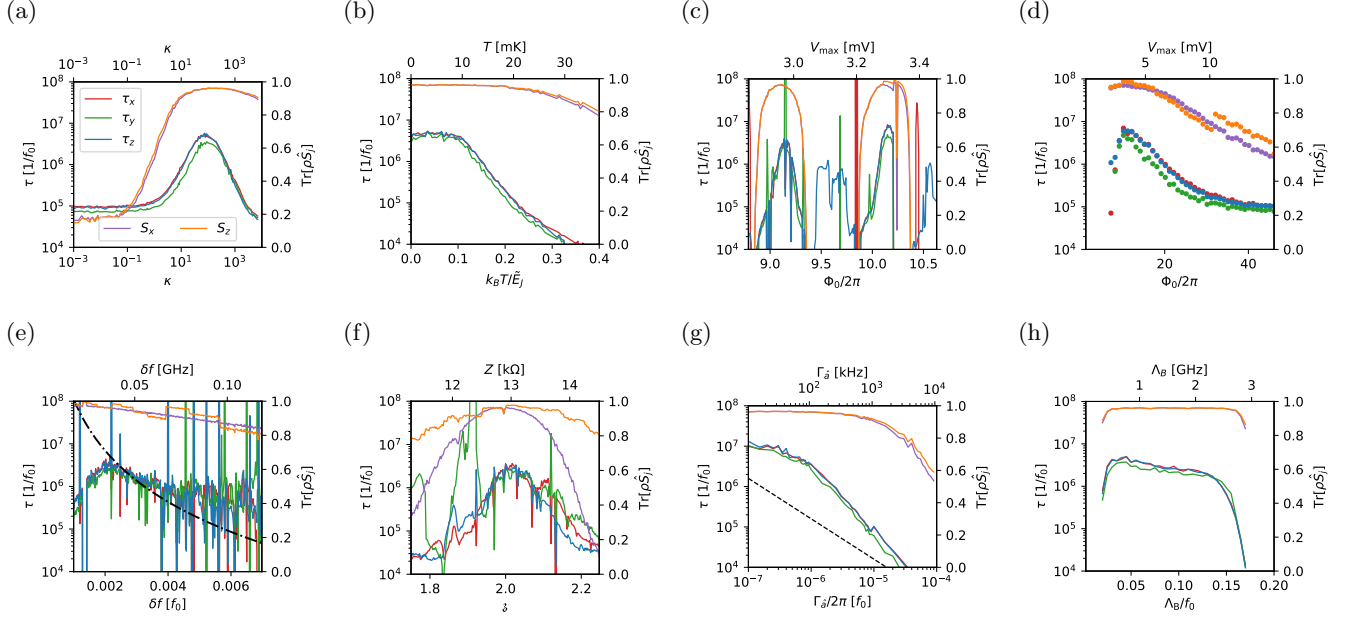


FIG. 8. **Qubit performance with low-pass filter approach** Lifetimes of information τ_j , $j = x, y, z$ stored in the expectation values of the logical operators $\langle \hat{\sigma}_j \rangle$, $j = x, y, z$ as a function of (a) dimensionless coupling to the filtered bath γ_B , (b) temperature (dashed line: Arrhenius law $\propto e^{2\tilde{J}/k_B T_E}$), (c) driving amplitude, (d) driving amplitude at maxima $\Phi_0 = 2\pi(z + \frac{1}{8})$, $z \in \mathbb{N}$, (e) detuning, (f) impedance, (g) photon loss rate $\Gamma_{\hat{a}}$, and (h) filter bandwidth Λ_B . The black dashed line in (g) is the photon loss rate $\Gamma_{\hat{a}}$ itself. We keep all non-varied parameter fixed at the default values in Table II. The upper x-axis is for a NbN resonator with $f_0 = 17$ GHz.